



PII S0016-7037(01)00749-9

On the formation of Fe-Ni metal in Renazzo-like carbonaceous chondrites

HAROLD C. CONNOLLY JR.,^{1,*} GARY R. HUSS,^{2,3} and G. J. WASSERBURG²¹California Institute of Technology, Division of Geological and Planetary Science, 100-23, Pasadena, CA 91125, USA²Lunatic Asylum, Charles Arms Laboratory, Division of Geological and Planetary Sciences, 170-25, California Institute of Technology, Pasadena, CA 91125, USA³Department of Geology and Center for Meteorite Studies, Arizona State University, P.O. Box 871404, Tempe, AZ 85287-1404, USA

(Received November 3, 2000; accepted in revised form July 12, 2001)

Abstract—The Fe-Ni metal within chondrites has been postulated to have originated either through condensation or as a byproduct of chondrule formation. To test these hypotheses, we studied metal in three Renazzo-like carbonaceous (CR2) chondrites from three petrographic settings: inside chondrules, on chondrule rims, and in the matrix. Abundances of Fe, Ni, Co, Cr, and P were determined in situ by electron microprobe, and those of Os, Ir, Pt, and Au were measured by a newly developed ion microprobe technique. The refractory platinum group elements Os, Ir, and Pt behave coherently in CR2 metal. They are either all enriched, all depleted, or unfractionated with respect to Fe and cosmic ratios. Metal with approximately CI Os/Fe, Ir/Fe, and Pt/Fe occur primarily in chondrule interiors. All metal grains have essentially CI values of Ni/Fe and Co/Fe. Almost all metal grains have lower-than-CI ratios of the volatile elements, Au and P. We also estimated the bulk compositions via analyses of phases and modal recombination of a subset of the chondrules whose metal we analyzed. The bulk compositions of chondrules are generally unfractionated relative to CI chondrites for elements more refractory than ~Cr but are depleted in more volatile elements. Abundances of siderophile elements correlate strongly with the metal abundance in the chondrules, which implies that siderophile depletions are due to expulsion of metal from the chondrule melts. The metal most likely originated during melting via reduction of oxides by C that was part of the chondrule precursor. During chondrule heating, molten metal efficiently extracted siderophile elements from the silicate melt. Rim metal consists of two types. One is like metal in chondrule interiors and was in the process of being expelled when the chondrules were quenched. The other shows systematic depletions in Os, Ir, and Pt relative to Fe and higher concentrations of Au and P than interior metal. This metal is attributed to recondensation from a vapor depleted in refractory siderophiles, a vapor most likely derived via evaporation from chondrules. Large, isolated matrix metal grains comprise the same two groups as rim grains and have the same origins. Bulk chondrule compositions and siderophile abundance patterns in metal indicate that the precursors of CR2 chondrules had CI-like abundances of refractory and moderately volatile elements but was likely depleted in the more volatile elements. Copyright © 2001 Elsevier Science Ltd

1. INTRODUCTION

The Renazzo-like carbonaceous chondrites (CR2) consist of chondrules, chondrule fragments, calcium-aluminum-rich inclusions (CAIs), dark inclusions, and metal and sulfide grains in a fine-grained phyllosilicate-dominated matrix (e.g., Weisberg et al., 1993). These meteorites have experienced little thermal metamorphism but have been affected by aqueous alteration to varying degrees. In most CR2 chondrites, the aqueous alteration was restricted to the matrix and the mesostasis of some chondrules; the larger ferromagnesian mineral grains and the metal and sulfide grains were not significantly affected (Weisberg et al., 1993). The majority of chondrules in CR2 chondrites are low-FeO type I chondrules (using the classification of Jones and Scott, 1989; Jones 1994) and exhibit porphyritic olivine (PO), porphyritic pyroxene (PP), and porphyritic olivine-pyroxene (POP) textures. These textures, combined with the lack of any identifiable relic grains within chondrules, suggest relatively simple formation histories.

The origin of Fe-Ni metal within CR2 chondrites has been

debated extensively. Some argue that the metal is the product of direct condensation from a gas of solar bulk composition before the formation of silicates (e.g., Weisberg et al., 1995). Others argue that metal was produced within chondrules via reduction of oxidized Fe within chondrules while they were molten (Kracher et al., 1983; Connolly et al., 1994; Zanda et al., 1994), with matrix metal grains originating within chondrules and expelled as immiscible liquids. Chondrules in CR2 chondrites can be interpreted as exhibiting all stages of metal expulsion. Another idea, presented by Lee et al. (1992), suggests that at least some of the metal within CR2 meteorites was produced by reduction of oxidized Fe during parent body metamorphism.

To effectively evaluate the validity of these ideas it is required that the compositions of the metal be determined in situ, maintaining the petrographic context of each grain. Until recently, such studies could only be conducted by means of the electron microprobe, limiting analyses to major (e.g., Fe and Ni) and minor element (Co, Cr, P, etc.). Important findings have resulted from such studies, but there are limitations. The Co/Ni ratio of metal grains has been argued to be a key indicator that the metal was condensed from a vapor. However, the volatilities of Fe, Co, and N are very similar (50% condensation temperatures of 1336, 1351, and 1354 K, respectively, at 10^{-4} atm; Wasson, 1985). It is risky at best to largely base a

* Author to whom correspondence should be addressed, at CUNY-Kingsborough, Department of Physical Sciences, 2001 Oriental Boulevard, Brooklyn, NY 11235 (vorlon@gps.caltech.edu).

model for metal origin on the difference of three degrees in the condensation temperature of two elements. In addition, the partitioning of these elements into Fe-Ni metal, whether between silicate liquid and metal or a gas and metal, is affected by the f_{O_2} (partial pressure of oxygen) experienced. Thus it cannot be determined uniquely if changes in Co/Ni ratios of metal grains reflect the condensation sequence or variation in partitioning between metal and silicate melt due to f_{O_2} fluctuations during metal formation within molten chondrules.

Highly siderophile trace elements provide another tool with which to study the origin of CR2 metal (Kong et al., 1999; Kong and Palme, 1999). However, instrumental neutron activation analysis, which is typically used for these studies, does not maintain the petrographic context of the metal grains. What is needed is an investigation of the highly siderophile trace elements at high spatial resolution in situ, maintaining the petrographic context of grains. Only recently has this become possible through either secondary ion mass spectrometry (SIMS) or laser ablation IC-PMS (Hsu et al., 1998a, 2000; Campbell and Humayun, 1999a, b). These techniques provide the concentrations of such elements as Os, Ir, Pt, and Au, which span a large range in condensation temperatures (Os = 1814 K, Ir = 1610 K, Pt = 1411 K, and Au = 1225 K; Wasson, 1985). At the conditions under which chondrules formed, the partitioning of these four siderophile elements between metal and silicate melt is insensitive to changes in f_{O_2} . Therefore, we argue that determining these highly siderophile trace elements along with minor elements in situ provides more critical data for evaluating the origin of metal.

We report on a combined SIMS–electron microprobe study of metal in chondrules, at chondrule rims, and in matrix in CR2 chondrites. We also present detailed major, minor, and trace-element data for the silicate phases on several of the chondrules from which metal was analyzed. These data, collected within their petrographic context, permit us to evaluate models for the origin of CR2 chondrite metal. The present study uses a new analytical procedure developed by Hsu et al. (1998a, 2000) for the analysis of Os, Ir, Pt, and Au in situ by SIMS. Preliminary reports of this investigation were presented by Connolly et al. (1998, 2000).

2. EXPERIMENTAL TECHNIQUES

2.1. Petrography

One thin section from each of three CR2 meteorites (PCA 91082,15, EET 92042,27, and Renazzo USNM 6226-3) was selected for study by optical and scanning electron microscopy. Backscattered electron images we used to produce a photomosaic of each section for careful examination. Modal mineral abundances for the chondrules were determined by point counting high-resolution, backscattered-electron images (minimum of 1000 points per chondrule) of individual chondrules. We selected chondrules with a range of bulk metal contents for detailed study, including some with extensive rim metal and some without. Some large isolated metal grains were also selected.

2.2. Electron Microprobe Analyses

Major- and minor-element analyses and backscattered-electron imaging were carried out on the JEOL 733 five-spectrometer electron microprobe at Caltech. Silicates and metal (plus one sulfide) were analyzed in separate runs by means of wavelength-dispersive spectrometers with an accelerating voltage of 15 kV and a beam current of 40 nA as measured in the Faraday cup. Counting times were 40 s for peak and

15 s for backgrounds. To ensure the accuracy of our analyses, wavelength scans were performed on several Fe-Ni metal grains to check peak and background spectrometer positions. Data were corrected by the CITZAF program (Armstrong, 1995). Checks were performed on the data reduction to ensure accuracy by using two different sets of published mass absorption coefficients and using other reduction programs accompanying the software of John Donovan, Probe for Windows, version 2.09. Detection limits in parts per million for minor elements in Fe-rich metal are as follows: 150 for Si, 210 for Cr, 220 for P, 230 for S, and 300 for Co. For silicates, the detection limits in parts per million are 100 for Na, 100 for K, 70 for Al, 120 for Ca, 260 for Ti, 290 for Cr, 210 for Mn, 240 for Fe, 200 for Ni, and 160 for Co.

2.3. Ion Probe Measurements

Ion probe measurements were carried out with PANURGE, a modified Cameca ims 3f ion microprobe. Measurements of Os, Ir, Pt, and Au in meteoritic metal were made by means of the technique described in Hsu et al. (1998a, 2000). A 10-nA Cs^+ primary beam was used to generate negative secondary ions of Fe, Co, Ni, Os, Ir, Pt, and Au. Molecular interferences were eliminated through a combination of 40 eV of energy filtering, which efficiently suppresses complex molecular ions, and a mass resolving power of ~ 1900 , sufficient to resolve the signals from various Cs-Fe and Cs-Ni compounds. Isotopic ratios ($^{188}\text{Os}/^{189}\text{Os}$, $^{192}\text{Os}/^{189}\text{Os}$, $^{191}\text{Ir}/^{193}\text{Ir}$, and $^{194}\text{Pt}/^{195}\text{Pt}$) were monitored to assure that only platinum group elements (PGEs) ions were being counted (a small correction is required for ^{192}Pt on ^{192}Os). Standards used were Bugoslavka (hexahedrite), Tocopilla (hexahedrite), and Santa Clara (ataxite), all of which have well determined abundances of Os, Ir, Pt, and Au.

Ion probe measurements of PGEs in metal can exhibit large variations in ion yield. The ion yield variations, however, are correlated and can be monitored by means of the Fe ion yield (Hsu et al., 2000). The data reported here were collected with the same instrumental setup and standardization as those of Hsu et al. (2000) and were reduced by means of the correlations shown in figure 2 of that article. Ion yields for most of our measurements on samples and standards were quite similar. For these measurements, uncertainties due to ion yield variations are not important. The biggest identifiable cause of increases in the ion yields seems to be the presence of oxygen-bearing phases in the sputtered volume. If the ion beam sputters through the metal in a thin section, the ion yield increases dramatically as the beam begins to sputter the glass. All measurements were truncated whenever such a sharp increase in ion yield was observed. For a few of our measurements, oxygen-bearing phases were present within the metal or the beam overlapped onto surrounding silicates resulting in much higher ion yields for Fe, Ni, Co, and Os. These measurements have larger uncertainties. Uncertainties for ion probe data reported in tables and figures are based on a 2σ counting uncertainty and incorporate uncertainties in the Fe ion yield, the slope of the ion-yield correlation, and a 10% uncertainty in the trace-element abundances in the three standards.

Rare earth elements (REE) and other trace elements in silicates were measured at low mass resolution using 80 eV of energy filtering to suppress the signals of complex molecular interferences and measured signals were deconvolved into REE and REE-oxide components (Zinner and Crozaz, 1986; Fahey et al., 1987). Calcium and Mg were used as reference elements. A synthetic Ti-pyroxene glass, NBS 612 glass, and Angra dos Reis pyroxene served as standards. Reported uncertainties (2σ) come from counting statistics and do not include the 5 to 10% uncertainties inherent in the abundance calibrations.

2.4. Bulk Compositions of Chondrules

Bulk compositions of the chondrules were estimated by converting the modal mineral abundances for each chondrule from volume percent to weight percent and then multiplying the weight fraction of each mineral by its major, minor, and trace-element concentrations. In calculating the bulk compositions, it was assumed that Os, Ir, Pt, Au, and P were all in the metal phase. There are significant unquantifiable uncertainties in the modal abundances due to sampling of chondrule minerals by the plane of the section. The uncertainties are most significant for small chondrules where a few mineral grains dominate. Two chondrules, PCA chondrule 8 medium sibling and EET chondrule

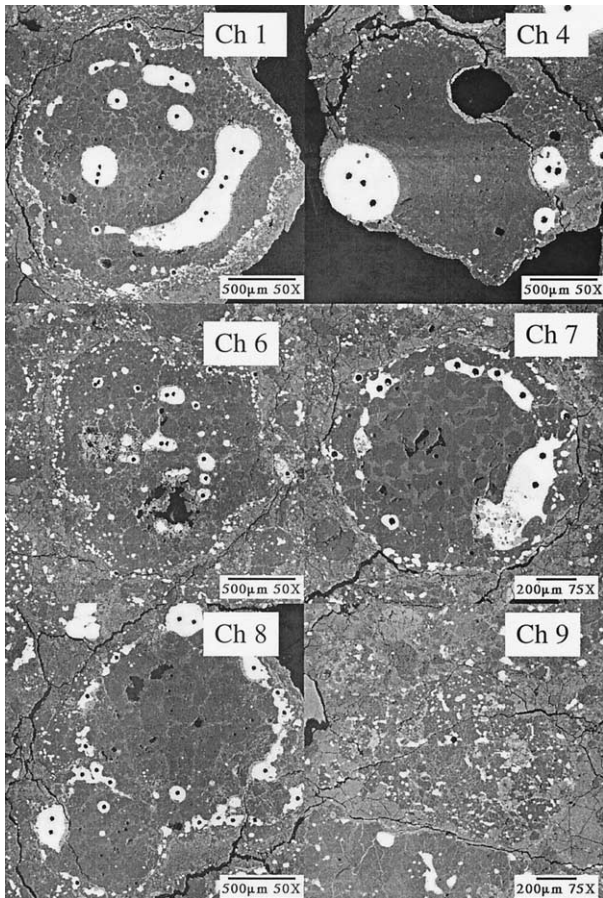


Fig. 1. Back-scattered electron images of investigated chondrules from PCA 91082. The abbreviation "Ch" followed by the number identify the chondrules. Note the scale bars. See Table 1 for a summary of the petrology.

3, show relative depletions of refractory lithophiles, sited mostly in the mesostasis, and relative enrichments in Mg and Si. This pattern suggests that our estimates are not representative of the true modal abundances. Uncertainties in metal abundances are also relatively large because the metal often resides in a handful of grains. These uncertainties are important to interpretations of bulk compositions. Additional uncertainties arise because the mesostasis of many chondrules is altered. A poorly chosen spot for mesostasis analysis can also potentially compromise the estimated bulk composition.

3. RESULTS

3.1. Petrology

The samples investigated were PCA 91082,15, EET 92042,27, and Renazzo USNM 6226-3 (hereafter PCA, EET, and Renazzo). All are typical of CR2 meteorites in petrography and degree of alteration, with Renazzo being the quintessential CR2. We selected five type 1 porphyritic chondrules and one fine-grained object (either a pyroxene-rich agglomeratic chondrule or an igneous rim fragment, chondrule 9) from PCA (Fig. 1), five porphyritic and one barred chondrule, all type I, from EET (Fig. 2), and four type I porphyritic chondrules from Renazzo (Fig. 3). The petrography of these chondrules is summarized in Table 1 and the modal mineral abundances are given in Table 2. The metal contents of these chondrules span the

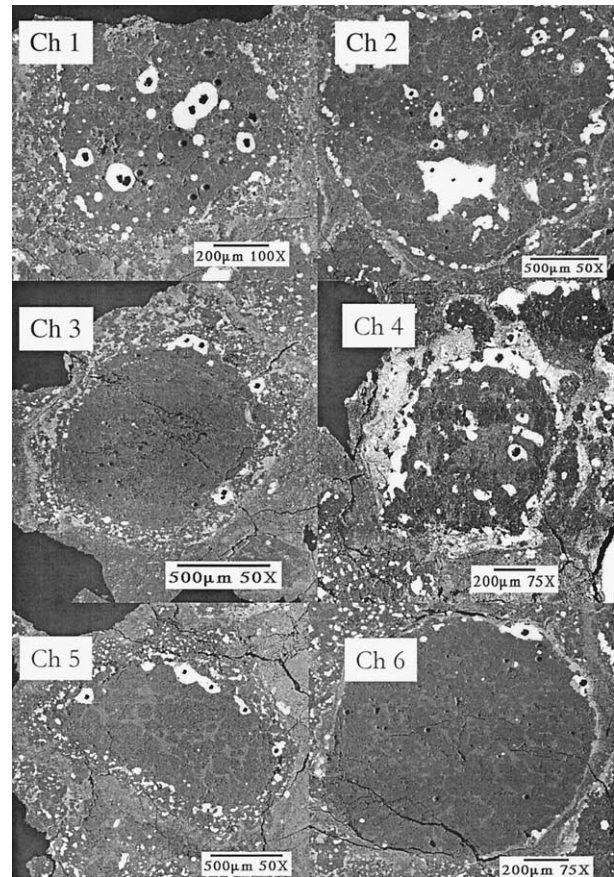


Fig. 2. Back-scattered electron images of investigated chondrules from EET 92042. Note the scale bars. See Table 1 for a summary of the petrology.

range observed in chondrules from CR2 chondrites. Some chondrules have metal and silicate rims that have undergone some melting (Figs. 1 to 3); however, there are no clearly defined layered rims as are often found on CR2 chondrules (Weisberg et al., 1993). The mesostases of the investigated chondrules are mixtures of glass and fine-grained phases. The fine-grained phases made an accurate quantitative characterization impossible, but EDS analysis and published studies suggest that they are mainly phyllosilicates. All chondrules were devoid of any apparent relict grains, as established by means of established criteria for their characterization (Nagahara, 1981; Rambaldi, 1981; Grossman et al., 1988; Jones, 1996; Jones and Danielson, 1997).

We distinguish three petrographic occurrences of metal grains in CR2 chondrites: (1) in the interiors of chondrules, (2) on chondrule rims, and (3) in the matrix. Our definition of rim metal is somewhat different than that used by Lee et al. (1992). Metal touching chondrule margins, whether partly on the interior or mainly around the outside margin, is defined here as rim metal. Texturally, many of the metal grains within the studied CR2 chondrules are rounded, with smooth outlines, but some grains actually conform to the shape of the surrounding silicates (Figs. 1 to 3). Rim metal occurs either as a thin zone of fine-grained, elongate metal grains (e.g., PCA chondrules 1 and 6 in Fig. 1; EET chondrule 1 in Fig. 2) or as rounded blebs (e.g.,

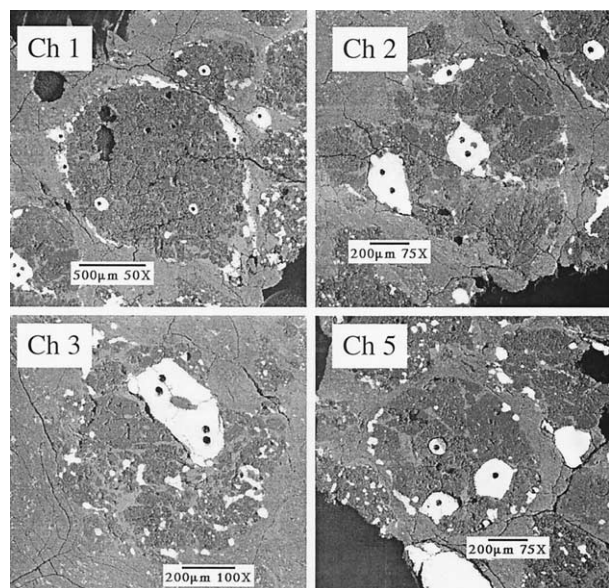


Fig. 3. Back-scattered electron images of investigated chondrules from Renazzo. Note the scale bars. See Table 1 for a summary of the petrology.

PCA chondrules 4 and 8 in Fig. 1). In some cases, both morphologies appear on the rim of the same chondrule (e.g., EET chondrule 3 in Fig. 2). Metal within the matrix occurs with a range of sizes and shapes. For this study, we chose large (hundreds of microns to slightly over a millimeter), isolated grains that are clearly outside of chondrules. These grains have rounded to subrounded shapes (Fig. 4). One matrix sulfide grain, which has an irregular shape and abraded edges, was also studied.

3.2. Composition of CR2 Metal

A total of 140 points was analyzed on 104 metal grains from the three sections. All metal grains from the matrix, chondrule rims, and all but five grains from chondrule interiors have Ni values between 4 and ~8 wt% (Tables 3 to 5). Grains from chondrule interiors tend to have higher Ni contents than rim grains, although the two distributions overlap significantly (Fig. 5). The highest Ni contents are observed in Renazzo chondrule 1 (10 to 12.7 wt%, Table 5) and in PCA chondrule 6 (7.5 to 13.3 wt%, Table 3). Renazzo chondrule 1 is metal poor (Fig. 3), but PCA chondrule 6 has a moderate amount of metal (Table 2). Cobalt and Ni contents are strongly correlated (Fig. 5a), with a tendency toward lower contents in rim grains (also see Lee et al., 1992; Weisberg et al., 1993). The Ni and Co contents of matrix grains span most of the range covered by rim and interior metal from chondrules but do not reach the extremes seen in Renazzo chondrule 1 and PCA chondrule 6 (Fig. 5a).

Chromium contents of the three petrographic types of metal cover essentially the same range, although the rim metal has a bimodal distribution (Fig. 5b). The highest Cr values (0.35 to 0.50 wt%) are found in rims of PCA chondrules 1, 7, and 8. Other rim grains from PCA, EET, and Renazzo have Cr contents below 0.25 wt%. There is no correlation between Cr and Ni content, and Cr/Ni ratios (0.02 to 0.11) are much lower than

Table 1. Summary of the petrology of investigated chondrules.^a

Sample	Textural type	Chemical type	Fa ^b	Igneous rim
PCA 91082,15				
Chondrule 1	PO	IA	1.91	Yes
Chondrule 4	PPO ^c	IAB	3.17	No
Chondrule 6	POP ^c	IAB	1.57	No
Chondrule 7	PO	IA	2.34	Yes
Chondrule 8L ^d	POP ^c	IAB	1.72	No
Chondrule 8M ^e	PO	IA	1.80	No
Chondrule 9	GP	IB		No
EET 92070,20				
Chondrule 1	POP	IAB	2.88	Yes
Chondrule 2	POP	IAB	2.95	No
Chondrule 3	BOP	IAB	3.22	Yes
Chondrule 4	PO	IA	2.05	Yes
Chondrule 5	POP	IAB	2.03	Yes
Chondrule 6	POP ^c	IAB	4.43	No
Renazzo USNM 6226-3				
Chondrule 1 ^f	POP	IAB	1.98	No
Chondrule 2	PP	IB		No
Chondrule 3	PP	IB		No
Chondrule 5	PP	IB		No

^a Textures: The nomenclature used here is after Gooding and Keil (1981). POP = porphyritic olivine pyroxene; PO = porphyritic olivine; PP = porphyritic pyroxene; GP = granular pyroxene; BOP = barred olivine pyroxene. In the naming of the textural types, the minerals are ordered according to decreasing modal abundance. Chemical type: Here we applied the chondrule classification system of Jones (1994, 1996), Jones and Scott (1989).

^b The Fa content is an average of at least three analyzed olivine grains, their cores only.

^c These chondrules have a poikilitic texture.

^d The larger chondrule of three-unit compound chondrule set.

^e The medium sibling compound chondrule from A.

^f This is the larger of a two-unit compound chondrule.

the solar value (2.42), reflecting the fact that most of the Cr in the chondrules is oxidized (see Discussion). Phosphorus and Au contents tend to be higher in rim metal than in either interior or matrix metal (Figs. 5c,d). Neither element correlates with Ni. Most grains from chondrule rims and interiors have Au contents no greater than ~0.5 ppm, although nine grains have higher values ranging up to 1.3 ppm. Most P/Ni and Au/Ni ratios are well below solar values, reflecting volatile loss from the bulk chondrules (see Discussion).

To understand fractionations of siderophile and potentially siderophile elements with respect to the bulk solar system composition, it is useful to use the ratio of the element concentrations to the Fe content of their host metal grain and then normalize to the same ratio for CI chondrites (e.g., sample Os/Fe normalized to CI Os/CI Fe). The metal data are plotted in this format in Figures 6 to 10. Although the metal grains exhibit considerable diversity, there are features that appear repeatedly.

The first important feature is the coherence of Os, Ir, and Pt. These elements are typically either all enriched, all depleted, or unfractionated with respect to cosmic ratios (Figs. 6 to 10). Large depletions of Os, Ir, and Pt tend to be associated with relative enrichments of Au and P (e.g., PCA chondrule 6 and 7, Fig. 6; EET chondrule 4, Fig. 8; Renazzo chondrule 1, Fig. 9; PCA matrix metal 2, 3, Fig. 10). Metal depleted in Os, Ir, and Pt tends to be located on the rims of chondrules. Metal with

Table 2. The modal abundances of phases within a selected subset of chondrules.^a

Sample	Olivine (wt%)	Mesostasis (wt%)	Low-Ca Pyx (wt%)	High-Pa Pyx (wt%)	Rim meta (wt%)	Interior metal (wt%)
PCA 91082,15						
Chondrule 1	46.85	8.29	1.94	0.14	9.76	34.96
Chondrule 7	47.24	9.60	2.00	1.53	6.22	33.42
Chondrule 8L	33.35	8.81	24.08	0.26	14.63	2.09
Chondrule 8M	71.01	4.13	4.57	1.88	16.77	1.57
EET 92042,20						
Chondrule 1	43.64	3.76	19.72	0.38	9.46	23.04
Chondrule 2	24.63	21.93	16.09	0.25	2.43	34.66
Chondrule 3	43.40	4.89	41.84	0.00	8.97	0.90
Chondrule 6	68.39	8.18	11.37	3.11	7.75	1.20
Renazzo USNM 6226-3						
Chondrule 1	51.79	4.52	26.94	1.77	11.83	3.15

^aChondrule 8L is the largest of the three that make up this compound chondrule. Chondrule 8M is the medium sibling of the compound chondrule 8. Only the interior metal abundance was used to calculate bulk compositions of chondrules.

approximately solar Os/Fe, Ir/Fe, and Pt/Fe occurs primarily in chondrule interiors, although variation from this generalization does exist (Figs. 6 to 9). Rim metal shows a range of Os/Fe, Ir/Fe, and Pt/Fe ratios, but in most grains, these ratios are lower than the CI ratios.

The second important observation is that Cr, Au, and P are systematically depleted relative to the CI ratios (Figs. 6 to 10). As will be shown below, Cr partitions strongly into the silicates and its depletion reflects this partitioning. Gold and P are the most volatile elements measured in this study. Gold is depleted in bulk CR2 chondrites relative to refractory siderophile elements such as Os, Ir, Pt (Kallemeyn et al., 1994; Kong et al., 1999). Although bulk CR2 data is not available for P, we would expect that it is similarly depleted relative to refractory siderophile elements. The magnitude of the depletions for Au and P are variable and tend to anticorrelate with Os, Ir, and Pt (Figs. 6 to 10).

The third observation is that there is often a range of patterns within a single chondrule, characterized by Os, Ir, and Pt behaving coherently and often anticorrelating with Au and P (e.g., PCA chondrules 1 and 7; Fig. 6). This variability is more extreme in chondrules that are texturally complex, with rings of metal that seem to define earlier surfaces of the chondrules (e.g., PCA chondrules 1 and 7; Fig. 1). In a handful of cases, Os, Ir, and Pt appear to be fractionated from one another. These differences may reflect a complex melting history for the chondrules, a high degree of partial melting, or a volatility-controlled process (see Discussion). However, five analyses that apparently show higher abundances of Os and Ir relative to Pt also have unusually large ion-yield corrections (Fe ion yields of 0.010 to 0.028 compared with 0.002 to 0.004 counts/s/nAmp/ppm found in ~70% of the measurements). For these five grains, the fractionations may well be experimental artifacts. They all from PCA: grain 20 of chondrule 1, grain 1 of chondrule 7, grain 8 of chondrule 8, and points 1 and 2 in matrix grain 6 (point 3, which shows a similar fractionation also had a higher than normal Fe ion yield).

One isolated matrix sulfide grain was measured. It has Ni/Fe and Co/Fe ratios roughly two times higher than CI ratios. Os, Ir, and Pt are highly depleted relative to CI ratios and their abundances are given as upper limits in Table 3. Chromium, Au, and P are also somewhat more depleted relative to CI ratios

than in metal grains. Appropriate ion-probe sensitivity factors were not available, so the Au abundance has some additional analytical uncertainty. The low abundances of Os, Ir, and Pt in the investigated troilite grain are consistent with previous work (e.g., Shen et al., 1996) and show that these elements are not compatible in troilite.

3.3. Silicate Mineral Compositions

The average compositions of chondrule silicate phases are listed in Table 6. Olivine and Ca-poor pyroxene generally occur as euhedral crystals and are FeO-poor (Fa_{1.3-4.4}; Fs_{1.1-4.6} Wo_{0.9-0.6}). They exhibit the subtle zoning toward more Fe-rich compositions at crystal edges typical of type I chondrule phenocrysts. Fine crystals of Ca-rich pyroxene occur within the chondrule mesostasis as overgrowths on olivine or Ca-poor pyroxene crystals (Table 6). Chromium contents of olivine and pyroxene are at the high end of the range exhibited by these minerals in chondrites (cf. Brearley and Jones, 1998). The mesostasis of chondrules is often altered to fine-grained phases likely composed of feldspars and phyllosilicates (Weisberg et al., 1993). Where possible, we analyzed glass compositions (Table 6), although the small size of some areas made them difficult to analyze. Renazzo chondrules were the most altered. Thus, for two of four investigated Renazzo chondrules (2 and 3) we report no mesostasis composition. Mesostasis compositions that we do report are typical for type I chondrules (Jones and Scott, 1989; Jones, 1994).

3.4. Bulk Compositions of Chondrules

To provide a framework for interpreting the metal data, we have estimated the bulk compositions of four chondrules each from PCA and EET and one chondrule from Renazzo (Table 7). The results are plotted normalized to CI chondrites in Figures 11 to 13. To a first approximation, all of the chondrules show refractory lithophiles are essentially unfractionated. Furthermore, the absolute abundances of these elements are essentially cosmic for all but one of the chondrules (EET chondrule 2, Fig. 12). Elements more volatile than Cr are systematically depleted in all chondrules. Superimposed on this general pattern are some correlated anomalies that differ in magnitude from chon-

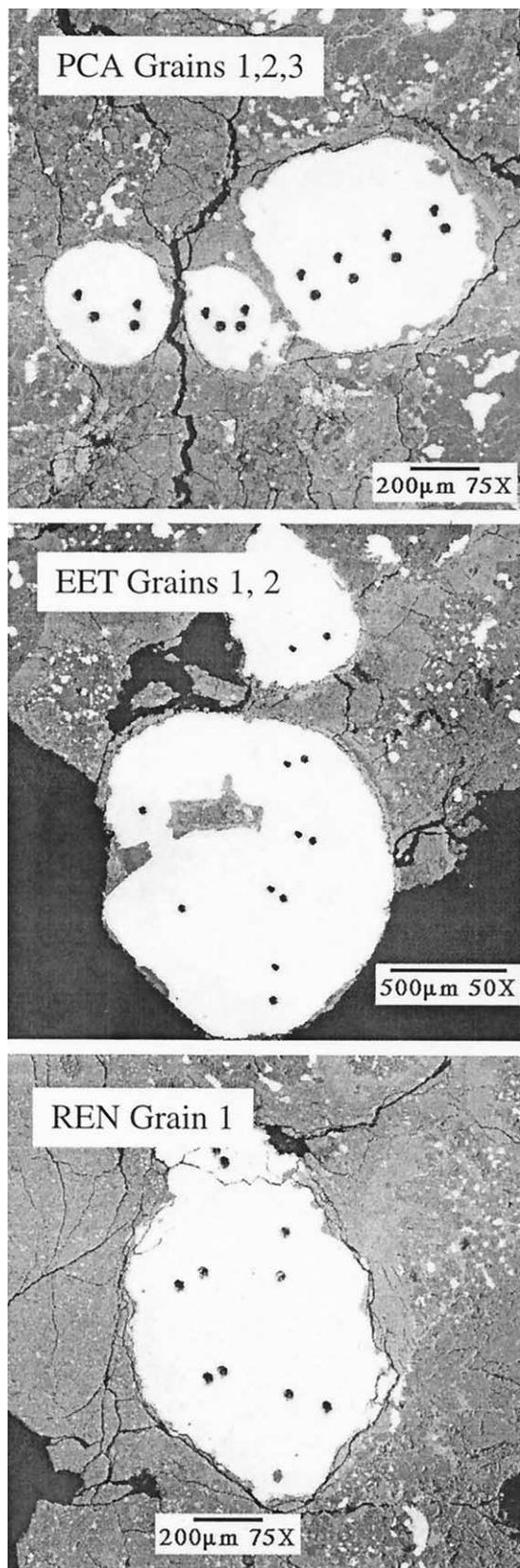


Fig. 4. Back-scattered electron images of representative isolated Fe-Ni matrix grains from the three meteorites we investigated. Note that their texture suggests that they were once molten.

drule to chondrule. For example, the Os, Ir, and Pt are present in their cosmic abundances in some chondrules, but in others all are depleted relative to cosmic abundances. Chondrules with large relative depletions of Os, Ir, Pt, Fe, Ni, Co, Au, and P (e.g., EET chondrules 2, 3, and 6, Renazzo chondrule 1) have lower than average metal contents (Table 2; Figs. 11 to 13); EET chondrules 3 and 6 have almost no interior metal (cf. Figs. 2 and 12). Anomalies in other elements (e.g., Ti) are due in part to the fact that analyses of one or more mineral phases are less than ideal. For example, EET chondrules 1 and 3 show small Ti depletions, which are likely an artifact of poor clinopyroxene analyses. Jagged REEs patterns in several chondrules and the large depletions of Ba and Sr in Renazzo chondrule 1 probably reflect our inability to get good analyses of the mesostasis in these chondrules.

4. DISCUSSION

4.1. Metal, Bulk Compositions, and Fractionations within CR2 Chondrules

The typical rounded forms and igneous textures show that the chondrules studied here crystallized from molten droplets. Metal grains within chondrules either have rounded forms or are interstitial to phenocrysts, occasionally conforming to silicate crystal boundaries (Figs. 1 to 3). These textures show that the metal existed as an immiscible liquid within the molten chondrules while they were crystallizing. Rounded-metal grains with their surface-tension-controlled forms solidified before much of the silicate liquid had crystallized. Metal grains that are interstitial to, and conform to, chondrule phenocrysts were shaped by the growing silicates. Thus, regardless of the origins of the metal, which will be explored below, all the metal was molten while chondrules were molten. This fact constrains the minimum temperature of the molten chondrules. The liquidus temperatures of Fe-Ni metal with ≤ 10 wt% Ni are 1783 to 1811K and solidus temperatures are only a few degrees lower at 1 atm (Swartzendruber et al., 1991). Thus, the evidence that chondrule metal was once molten shows that chondrules were heated to at least 1783K.

The conclusion that metal within chondrules was molten while the chondrules were liquid implies that siderophile elements should have partitioned strongly into the metal, in agreement with what is observed. Many metal grains from the interiors of chondrules have Os/Fe, Ir/Fe, Pt/Fe, Ni/Fe, and Co/Fe ratios that cluster around CI values, with lower-than-CI ratios for Cr/Fe, Au/Fe, and P/Fe (Figs. 6 to 9). The bulk compositions of the chondrules also show that metal controls the abundance of siderophile elements in these objects. Chondrules with high metal contents have high abundances of siderophile elements (cf. Figs. 1 to 3 and Figs. 11 to 13). Chondrules that are metal poor are depleted in siderophile elements, regardless of volatility (Figs. 11 to 13).

Some metal grains on the rims of chondrules and in the matrix have siderophile element abundances essentially the same as grains found within chondrules. During melting experiments designed to simulate chondrule formation, it was found that metal migrates to the surfaces of the charges due to surface tension effects (Planner, 1986; Connolly et al., 1994). Metal grains on chondrule rims and in the matrix with compositions similar to interior metal are most plausibly originally from

Table 3. Major, minor, and trace element concentrations of metal grains from chondrules and matrix of PCA91082,15.^a

Sample	Rim or interior	Os $\pm 2\sigma$ (ppm)	Ir $\pm 2\sigma$ (ppm)	Pt $\pm 2\sigma$ (ppm)	Ni ^b (wt%)	Co ^b (wt%)	Fe ^b (wt%)	Cr ^b (wt%)	Au $\pm 2\sigma$ (ppm)	P ^b (wt%)	Co/Ni
Chondrule I											
Grain 7	R	0.74 \pm 0.91	0.64 \pm 0.09	1.27 \pm 0.13	4.77	0.33	94.73	0.40	0.23 \pm 0.03	0.35	0.069
Grain 8-1	I	2.29 \pm 0.57	2.21 \pm 0.22	3.84 \pm 0.38	5.29	0.34	95.66	0.40	0.21 \pm 0.02	0.30	0.064
Grain 8-2	I	1.31 \pm 0.94	1.59 \pm 0.16	2.88 \pm 0.29	4.97	0.34	93.94	0.41	0.10 \pm 0.01	0.11	0.068
Grain 10	I	6.95 \pm 1.72	6.49 \pm 0.65	10.12 \pm 1.01	6.62	0.39	93.11	0.32	0.13 \pm 0.02	0.31	0.059
Grain 11	I	1.69 \pm 0.86	1.92 \pm 0.19	3.17 \pm 0.32	6.39	0.39	92.88	0.40	0.12 \pm 0.01	0.27	0.061
Grain 12	R	6.02 \pm 1.20	5.78 \pm 0.58	8.27 \pm 0.83	5.27	0.34	94.78	0.48	0.28 \pm 0.03	0.27	0.065
Grain 13	R	6.16 \pm 1.23	5.57 \pm 0.56	8.51 \pm 0.85	5.25	0.33	95.06	0.46	0.30 \pm 0.03	0.27	0.063
Grain 14	R	0.30 \pm 0.28	0.37 \pm 0.06	0.47 \pm 0.05	5.12	0.32	95.54	0.43	0.24 \pm 0.03	0.32	0.063
Grain 8-3	I	1.48 \pm 0.56	1.62 \pm 0.16	3.08 \pm 0.31	4.97	0.36	94.69	0.42	0.14 \pm 0.02	0.29	0.072
Grain 16	I	1.46 \pm 0.73	1.62 \pm 0.16	2.82 \pm 0.28	6.73	0.43	93.10	0.32	0.13 \pm 0.02	0.34	0.064
Grain 17-1	I	4.35 \pm 0.95	3.86 \pm 0.39	5.62 \pm 0.56	5.14	0.37	94.80	0.30	0.12 \pm 0.02	0.18	0.072
Grain 18	I	2.02 \pm 0.75	2.06 \pm 0.21	4.74 \pm 0.47	5.20	0.37	94.69	0.33	0.12 \pm 0.01	0.16	0.071
Grain 19	R	0.98 \pm 0.49	1.24 \pm 0.12	2.22 \pm 0.22	4.69	0.33	94.97	0.45	0.25 \pm 0.03	0.32	0.070
Grain 20	I	2.37 \pm 0.68	2.01 \pm 0.23	3.48 \pm 0.35	5.77	0.38	94.24	0.30	0.08 \pm 0.01	0.09	0.066
Grain 17-2	I	3.98 \pm 0.80	3.56 \pm 0.36	5.36 \pm 0.54	5.14	0.33	94.86	0.37	0.10 \pm 0.01	0.18	0.064
Grain 22	I	1.22 \pm 0.50	1.42 \pm 0.14	2.24 \pm 0.22	5.26	0.39	95.01	0.28	0.08 \pm 0.01	0.12	0.074
Grain 23	I	0.38 \pm 0.17	0.57 \pm 0.06	1.24 \pm 0.12	5.52	0.37	93.60	0.34	0.06 \pm 0.01	0.15	0.067
Chondrule 4											
Grain 3-1	R	1.50 \pm 0.56	1.20 \pm 0.12	2.20 \pm 0.22	5.67	0.39	94.99	0.19	0.26 \pm 0.03	0.27	0.069
Grain 3-2	R	1.31 \pm 0.35	1.34 \pm 0.13	2.21 \pm 0.22	5.67	0.39	94.99	0.19	0.26 \pm 0.03	0.27	0.069
Grain 5	R	0.15 \pm 0.40	0.22 \pm 0.03	0.42 \pm 0.04	5.41	0.35	95.16	0.18	0.25 \pm 0.03	0.26	0.065
Grain 6	R	0.13 \pm 0.23	0.11 \pm 0.01	0.28 \pm 0.03	5.63	0.36	94.50	0.20	0.31 \pm 0.03	0.28	0.064
Grain 7	R	1.52 \pm 0.35	1.45 \pm 0.15	2.38 \pm 0.24	4.88	0.30	94.40	0.13	0.27 \pm 0.03	0.27	0.061
Chondrule 6											
Grain 5	I	2.05 \pm 0.41	2.02 \pm 0.20	4.14 \pm 0.41	8.86	0.49	90.32	0.28	0.16 \pm 0.02	0.24	0.055
Grain 6	I	3.57 \pm 0.71	3.03 \pm 0.30	4.95 \pm 0.49	7.54	0.43	92.64	0.32	0.14 \pm 0.02	0.27	0.057
Grain 7	I	2.22 \pm 0.69	2.55 \pm 0.25	5.08 \pm 0.51	7.55	0.45	92.52	0.31	0.14 \pm 0.02	0.29	0.060
Grain 8	I	1.74 \pm 0.47	1.92 \pm 0.19	4.24 \pm 0.42	7.65	0.45	91.87	0.28	0.12 \pm 0.01	0.28	0.059
Grain 9	I	3.67 \pm 1.13	3.51 \pm 0.35	5.75 \pm 0.57	7.78	0.44	89.42	0.31	0.14 \pm 0.02	0.25	0.057
Grain 10	I	3.53 \pm 0.91	3.85 \pm 0.39	8.80 \pm 0.88	13.39	0.64	85.49	0.31	0.13 \pm 0.02	0.32	0.048
Grain 11	I	2.00 \pm 0.50	2.21 \pm 0.22	4.41 \pm 0.44	7.65	0.43	91.34	0.29	0.13 \pm 0.02	0.25	0.056
Grain 12	R	1.03 \pm 0.35	0.87 \pm 0.09	1.67 \pm 0.17	4.87	0.36	95.24	0.12	0.43 \pm 0.05	0.44	0.074
Grain 14	R	<0.13	0.14 \pm 0.02	0.70 \pm 0.07	4.56	0.36	94.46	0.20	0.37 \pm 0.04	0.39	0.079
Grain 15	R	<0.10	0.08 \pm 0.02	0.26 \pm 0.03	4.56	0.31	94.53	0.17	0.23 \pm 0.03	0.42	0.068
Chondrule 7											
Grain 1	R	0.56 \pm 0.20	0.43 \pm 0.06	0.67 \pm 0.07	4.82	0.33	94.34	0.35	0.30 \pm 0.04	0.45	0.068
Grain 2-1	I	0.63 \pm 0.33	0.78 \pm 0.08	1.74 \pm 0.17	6.38	0.42	93.19	0.36	0.10 \pm 0.01	0.23	0.066
Grain 2-2	I	1.17 \pm 0.23	1.15 \pm 0.12	2.24 \pm 0.22	6.65	0.41	93.22	0.37	0.11 \pm 0.01	0.23	0.062
Grain 4-1	I	1.35 \pm 0.83	1.21 \pm 0.12	1.95 \pm 0.20	6.07	0.42	93.61	0.38	0.14 \pm 0.02	0.21	0.069
Grain 4-2	I	0.86 \pm 0.94	1.02 \pm 0.10	1.99 \pm 0.20	6.00	0.37	93.43	0.30	0.15 \pm 0.02	0.23	0.062
Grain 6-1	I	7.08 \pm 1.42	6.34 \pm 0.63	9.25 \pm 0.93	5.71	0.37	94.64	0.35	0.11 \pm 0.01	0.36	0.065
Grain 7	R	<.21	0.20 \pm 0.05	1.00 \pm 0.10	4.86	0.32	94.07	0.36	0.43 \pm 0.05	0.48	0.066
Grain 8	R	0.62 \pm 0.33	0.61 \pm 0.06	1.22 \pm 0.12	4.82	0.33	94.34	0.35	0.25 \pm 0.03	0.46	0.068
Grain 9	I	1.39 \pm 0.47	1.70 \pm 0.17	3.04 \pm 0.30	6.10	0.37	93.51	0.34	0.14 \pm 0.02	0.21	0.061
Grain 6-2	I	5.68 \pm 1.14	5.34 \pm 0.53	8.83 \pm 0.88	5.71	0.37	94.64	0.35	0.12 \pm 0.01	0.36	0.065
Grain 11-1	I	0.47 \pm 0.73	0.67 \pm 0.07	1.50 \pm 0.15	5.90	0.37	91.49	0.37	0.14 \pm 0.02	0.21	0.063
Grain 11-2	I	0.52 \pm 0.48	0.77 \pm 0.08	1.67 \pm 0.17	5.96	0.44	93.29	0.33	0.13 \pm 0.01	0.22	0.074
Chondrule 8											
Large Sibling											
Grain 4	R	3.76 \pm 0.75	4.74 \pm 0.47	15.75 \pm 1.58	5.08	0.32	92.21	0.44	0.12 \pm 0.01	0.30	0.063
Grain 5	R	0.86 \pm 0.95	1.03 \pm 0.10	5.26 \pm 0.53	5.15	0.34	91.86	0.38	0.14 \pm 0.02	0.28	0.066
Grain 7	I	2.66 \pm 0.91	2.53 \pm 0.25	4.51 \pm 0.45	7.50	0.45	92.30	0.38	0.09 \pm 0.01	0.18	0.060
Grain 8	R	0.77 \pm 0.31	0.67 \pm 0.07	1.18 \pm 0.12	4.93	0.32	94.19	0.39	0.19 \pm 0.02	0.41	0.065
Grain 12	R	0.77 \pm 0.84	0.92 \pm 0.09	1.27 \pm 0.13	5.23	0.34	92.25	0.48	0.13 \pm 0.02	0.33	0.065
Grain 13-1	R	3.07 \pm 1.57	3.20 \pm 0.32	4.95 \pm 0.49	5.29	0.36	91.86	0.49	0.12 \pm 0.01	0.33	0.068
Grain 13-2	R	2.58 \pm 1.48	2.75 \pm 0.28	4.45 \pm 0.45	5.29	0.36	91.86	0.49	0.12 \pm 0.01	0.33	0.068
Grain 17	R	0.41 \pm 0.33	0.66 \pm 0.07	1.17 \pm 0.12	4.98	0.34	92.66	0.46	0.12 \pm 0.01	0.33	0.068
Grain 18	R	0.95 \pm 0.54	0.84 \pm 0.08	1.56 \pm 0.16	4.83	0.31	92.94	0.42	0.19 \pm 0.02	0.32	0.064
Grain 19	R	0.94 \pm 1.05	1.11 \pm 0.11	2.07 \pm 0.21	4.27	0.29	92.87	0.35	0.22 \pm 0.02	0.46	0.068
Grain 20	R	0.68 \pm 0.41	1.01 \pm 0.10	1.87 \pm 0.19	4.77	0.32	92.66	0.42	0.13 \pm 0.02	0.40	0.067
Grain 21	R	0.35 \pm 0.19	0.55 \pm 0.06	1.17 \pm 0.12	5.09	0.32	93.10	0.40	0.12 \pm 0.01	0.36	0.063
Chondrule 8											
Medium Sibling											
Grain 1-1	R	2.24 \pm 0.80	2.60 \pm 0.26	4.54 \pm 0.45	5.55	0.34	93.29	0.44	0.09 \pm 0.01	0.32	0.061
Grain 1-2	R	3.18 \pm 0.52	2.97 \pm 0.30	5.63 \pm 0.56	5.55	0.34	93.29	0.44	0.13 \pm 0.02	0.32	0.061
Grain 3	I	6.28 \pm 1.26	6.39 \pm 0.64	10.01 \pm 1.00	7.90	0.37	90.53	0.38	0.19 \pm 0.02	0.22	0.047
Grain 15	R	0.16 \pm 0.35	0.39 \pm 0.04	1.32 \pm 0.13	4.68	0.30	94.28	0.39	0.18 \pm 0.02	0.37	0.064

(Continued)

Table 3. (Continued)

Sample	Rim or interior	Os $\pm 2\sigma$ (ppm)	Ir $\pm 2\sigma$ (ppm)	Pt $\pm 2\sigma$ (ppm)	Ni ^b (wt%)	Co ^b (wt%)	Fe ^b (wt%)	Cr ^b (wt%)	Au $\pm 2\sigma$ (ppm)	P ^b (wt%)	Co/Ni
Chondrule 8		Small Sibling									
Grain 9	R	0.45 \pm 0.15	0.41 \pm 0.06	1.35 \pm 0.13	4.97	0.35	94.12	0.38	0.21 \pm 0.03	0.38	0.070
Grain 10	R	<0.24	0.05 \pm 0.02	0.23 \pm 0.02	4.84	0.35	94.08	0.46	0.18 \pm 0.02	0.37	0.072
Grain 11	R	0.39 \pm 0.69	0.75 \pm 0.08	1.69 \pm 0.17	5.21	0.33	92.24	0.45	0.20 \pm 0.02	0.38	0.063
Grain 16	R	0.40 \pm 0.38	0.51 \pm 0.06	1.46 \pm 0.15	4.81	0.34	95.48	0.44	0.18 \pm 0.02	0.37	0.071
Chondrule 9											
Grain 1	I	0.44 \pm 0.20	0.45 \pm 0.05	0.89 \pm 0.09	5.22	0.37	93.52	0.51	0.21 \pm 0.02	0.36	0.071
Grain 1	I	0.56 \pm 0.31	0.60 \pm 0.08	1.11 \pm 0.11	5.22	0.37	93.52	0.51	0.19 \pm 0.03	0.36	0.071
Matrix grain 1											
Point 5		1.06 \pm 0.51	1.39 \pm 0.14	2.99 \pm 0.30	5.76	0.35	93.31	0.44	0.14 \pm 0.02	0.24	0.061
Point 6		1.30 \pm 0.31	1.47 \pm 0.15	3.34 \pm 0.33	5.20	0.38	93.93	0.42	0.11 \pm 0.01	0.30	0.073
Point 7		2.63 \pm 0.69	2.60 \pm 0.26	4.41 \pm 0.44	5.98	0.36	92.36	0.55	0.13 \pm 0.01	0.25	0.060
Point 8		1.17 \pm 0.52	1.82 \pm 0.18	3.55 \pm 0.36	4.46	0.36	94.44	0.39	0.13 \pm 0.02	0.23	0.078
Matrix grain 2											
Point 3		0.42 \pm 0.46	0.57 \pm 0.06	1.38 \pm 0.14	4.95	0.37	94.29	0.37	0.11 \pm 0.01	0.31	0.075
Point 4		0.62 \pm 0.51	0.52 \pm 0.06	1.33 \pm 0.13	5.06	0.35	94.46	0.36	0.13 \pm 0.02	0.30	0.069
Matrix grain 3											
Point 3		0.16 \pm 0.26	0.27 \pm 0.04	0.58 \pm 0.06	6.04	0.32	92.34	0.50	0.12 \pm 0.02	0.30	0.053
Point 4		0.26 \pm 0.35	0.38 \pm 0.05	0.66 \pm 0.07	5.07	0.37	93.42	0.40	0.13 \pm 0.02	0.25	0.073
Matrix grain 6											
Point 1		1.75 \pm 0.73	1.12 \pm 0.17	2.41 \pm 0.24	7.44	0.43	91.75	0.17	0.27 \pm 0.03	0.19	0.058
Point 2		2.20 \pm 0.53	1.65 \pm 0.17	3.15 \pm 0.31	7.44	0.43	91.75	0.17	0.19 \pm 0.02	0.19	0.058
Point 3		3.02 \pm 0.87	2.13 \pm 0.21	3.78 \pm 0.38	7.54	0.43	91.68	0.16	0.20 \pm 0.02	0.18	0.057
Matrix sulfide											
Point 1		<0.058	<0.005	<0.001	7.85	0.43	55.54	0.03	0.09 \pm 0.01	0.03	0.055
CI value		0.486	0.481	0.990	1.10	0.502	19.04	0.145	0.122	0.046	

^a The grain number in some cases is followed by a dash and another number (e.g., grain 3-2); this indicates that grain 3 was analyzed in more than one location (e.g., in 3-2, the 2 is spot 2).

^b Approximate 2σ errors: Ni = ± 0.10 ; Co = ± 0.04 ; Fe = ± 0.38 ; Cr = ± 0.04 ; P = ± 0.04 .

chondrule interiors. Grains on chondrule rims were trapped at the chondrule surfaces during the process of being expelled and those that were expelled formed matrix metal. We note that expulsion of metal from chondrule melts may provide a mechanism to initiate the metal-silicate fractionations that characterize different classes of chondritic meteorites (e.g., Larimer and Anders, 1970).

Essentially, all interior metal grains have lower-than-CI ratios of Cr/Fe, Au/Fe, and P/Fe (Figs. 6 to 9). Although Cr is depleted in metal grains, it is approximately at its CI abundance in bulk chondrule compositions. Thus, the Cr depletion reflects that fact that it partitions preferentially into the silicates. Gold and P, however, are depleted with respect to CI abundances in bulk chondrules (Figs. 11 to 13). Similarly, all chondrules are also depleted relative to CI in lithophile elements more volatile than Cr. The observed volatile depletions could have originated in two ways: (1) loss during chondrule melting, or (2) the precursor material that became the CR2 chondrites was already depleted in volatile elements before chondrule heating. Temperatures of >1783 K indicated by the molten metal in chondrules are well above the vaporization temperatures of most of the constituent elements, so some evaporation must have occurred. How much evaporation took place is not clear, but the relatively smooth depletion patterns with respect to volatility indicate that chondrules solidified before all of the volatiles were lost. We will argue below that rim metal grains enriched in Au and P with respect to interior grains consist of siderophiles that evaporated from the chondrules while they were molten and then recondensed onto chondrule surfaces. If

this is true, and if the bulk compositions of the chondrules were as volatile rich as CI chondrites, then one might expect the Au/F and P/Fe ratios to be higher than CI. The fact that they are lower implies that the precursor material was already depleted in volatile elements. The unfractionated abundances of the more refractory elements (except the siderophiles discussed above) imply that the precursor material had CI abundances in these elements.

4.2. Origin of Metal within CR2 Chondrules

Some of the metal in CR2 chondrules might have been inherited from chondrule precursor material. Such relict metal grains might retain anomalous siderophile-element contents inherited from their site of origin. For example, metal grains that started to condense at very high temperatures from a gas of solar composition and did not equilibrate with the gas at low temperatures might contain very high abundances of refractory PGEs. However, if the metal melted or equilibrated with the chondrule, this record of its prehistory would have been lost. Some chondrules show quite variable siderophile-element patterns (e.g., PCA chondrules 1 and 7) that could be interpreted as potential relict metal grains. However, the observed patterns are within the range seen in more homogeneous metal from other chondrules, implying that the metal formed by a similar process. In addition, chondrules with variable siderophile-element patterns appear on textural grounds to have had a complex, multistage melting history. If later melting events were not complete, permitting the metal to be homogenized, metal

Table 4. Major, minor, and trace element concentrations of metal grains from chondrules and matrix EET92042,20.^a

Sample	Rim or interior	Os $\pm 2\sigma$ (ppm)	Ir $\pm 2\sigma$ (ppm)	Pt $\pm 2\sigma$ (ppm)	Ni ^b (wt%)	Co ^b (wt%)	Fe ^b $\pm 2\sigma$ (wt%)	Cr ^b (wt%)	Au $\pm 2\sigma$ (ppm)	P ^b (wt%)	Co/Ni
Chondrule 1											
Grain 5	I	4.15 \pm 1.11	4.32 \pm 0.43	7.24 \pm 0.72	8.20	0.35	90.51 \pm 0.36	0.23	0.18 \pm 0.02	0.25	0.043
Grain 6	I	1.99 \pm 0.40	1.80 \pm 0.18	3.38 \pm 0.34	7.66	0.34	89.56 \pm 0.36	0.19	0.43 \pm 0.04	0.33	0.044
Grain 7	I	0.45 \pm 0.15	0.62 \pm 0.08	1.92 \pm 0.19	8.07	0.29	89.91 \pm 0.36	0.18	0.19 \pm 0.02	0.30	0.036
Chondrule 2											
Grain 3-1	I	1.45 \pm 0.43	1.65 \pm 0.16	3.18 \pm 0.32	6.43	0.34	92.29 \pm 0.36	0.18	0.18 \pm 0.02	0.18	0.053
Grain 3-2	I	1.53 \pm 0.46	1.80 \pm 0.18	3.61 \pm 0.36	6.82	0.35	92.62 \pm 0.38	0.26	0.17 \pm 0.02	0.15	0.051
Grain 5	I	1.36 \pm 0.43	1.93 \pm 0.19	3.81 \pm 0.38	6.88	0.30	91.34 \pm 0.36	0.10	0.17 \pm 0.02	0.15	0.044
Grain 6	I	1.37 \pm 0.97	1.64 \pm 0.16	3.31 \pm 0.33	6.67	0.33	91.06 \pm 0.36	0.19	0.19 \pm 0.02	0.14	0.049
Grain 7	I	1.08 \pm 0.41	1.23 \pm 0.12	2.52 \pm 0.25	7.72	0.29	90.30 \pm 0.36	0.16	0.08 \pm 0.01	0.15	0.038
Grain 8	I	1.08 \pm 0.32	1.16 \pm 0.12	2.50 \pm 0.25	8.42	0.36	90.18 \pm 0.36	0.19	0.08 \pm 0.01	0.13	0.043
Grain 9	R	2.09 \pm 0.42	1.91 \pm 0.19	2.76 \pm 0.28	4.70	0.24	94.62 \pm 0.38	0.12	0.53 \pm 0.06	0.19	0.051
Grain 10	I	1.46 \pm 0.37	1.38 \pm 0.14	2.56 \pm 0.26	8.01	0.30	89.72 \pm 0.36	0.13	0.06 \pm 0.01	0.12	0.037
Grain 11	I	1.06 \pm 0.22	1.18 \pm 0.12	2.40 \pm 0.24	6.80	0.22	90.57 \pm 0.36	0.15	0.17 \pm 0.02	0.18	0.032
Chondrule 3											
Grain 3	R	<0.17	0.26 \pm 0.04	0.53 \pm 0.05	5.44	0.26	93.63 \pm 0.38	0.20	0.22 \pm 0.03	0.41	0.048
Grain 4	R	<0.34	0.20 \pm 0.03	0.37 \pm 0.04	5.55	0.25	93.34 \pm 0.36	0.18	0.33 \pm 0.04	0.37	0.045
Grain 5	R	<0.16	0.05 \pm 0.01	0.16 \pm 0.02	5.45	0.26	93.34 \pm 0.36	0.21	0.29 \pm 0.03	0.36	0.048
Chondrule 4											
Grain 1	R	0.41 \pm 0.40	0.48 \pm 0.05	1.14 \pm 0.11	5.37	0.27	92.93 \pm 0.36	0.20	0.31 \pm 0.03	0.39	0.050
Grain 2	I	2.71 \pm 0.54	2.57 \pm 0.26	5.01 \pm 0.50	6.60	0.34	90.68 \pm 0.36	0.26	0.09 \pm 0.01	0.22	0.052
Chondrule 5											
Grain 1-1	I	2.83 \pm 0.57	2.60 \pm 0.26	3.71 \pm 0.37	5.25	0.23	93.78 \pm 0.36	0.39	0.16 \pm 0.02	0.23	0.044
Grain 1-2	I	1.15 \pm 0.41	1.27 \pm 0.13	2.53 \pm 0.25	5.17	0.28	93.10 \pm 0.36	0.36	0.15 \pm 0.02	0.26	0.054
Grain 3	I	2.22 \pm 0.61	2.09 \pm 0.21	3.68 \pm 0.37	5.24	0.29	92.26 \pm 0.36	0.41	0.22 \pm 0.02	0.26	0.055
Grain 4	I	<0.16	0.09 \pm 0.02	0.28 \pm 0.03	5.62	0.25	93.73 \pm 0.36	0.37	0.13 \pm 0.02	0.26	0.044
Grain 5	I	0.69 \pm 0.65	0.83 \pm 0.08	1.21 \pm 0.12	5.24	0.27	93.57 \pm 0.36	0.37	0.16 \pm 0.02	0.28	0.052
Chondrule 6											
Grain 1	R	1.07 \pm 0.46	1.23 \pm 0.12	1.87 \pm 0.19	4.75	0.25	94.57 \pm 0.36	0.10	0.35 \pm 0.04	0.34	0.053
Grain 2	R	0.15 \pm 0.18	0.24 \pm 0.04	0.71 \pm 0.07	4.83	0.24	92.71 \pm 0.36	0.13	0.87 \pm 0.09	0.27	0.052
Matrix grain 1											
Point 5		2.07 \pm 0.51	1.91 \pm 0.19	2.98 \pm 0.30	6.53	0.33	91.79 \pm 0.36	0.22	0.09 \pm 0.01	0.22	0.051
Point 6		4.97 \pm 1.09	3.84 \pm 0.38	4.43 \pm 0.44	7.04	0.33	91.62 \pm 0.36	0.23	0.12 \pm 0.01	0.24	0.047
Point 7		1.27 \pm 1.33	1.52 \pm 0.15	3.80 \pm 0.38	7.21	0.32	90.69 \pm 0.36	0.26	0.09 \pm 0.01	0.18	0.044
Point 8		1.71 \pm 0.48	2.00 \pm 0.20	3.23 \pm 0.32	6.96	0.32	90.40 \pm 0.36	0.26	0.10 \pm 0.01	0.18	0.046
Point 9		3.34 \pm 0.79	2.93 \pm 0.29	4.00 \pm 0.40	7.43	0.31	91.69 \pm 0.36	0.24	0.09 \pm 0.01	0.22	0.042
Point 10		1.90 \pm 0.82	1.96 \pm 0.20	3.30 \pm 0.33	6.25	0.29	92.94 \pm 0.36	0.23	0.11 \pm 0.01	0.22	0.046
Matrix grain 2											
Point 3		0.65 \pm 0.85	0.80 \pm 0.08	2.08 \pm 0.21	4.58	0.23	94.21 \pm 0.36	0.24	0.31 \pm 0.03	0.28	0.050
Point 4		1.47 \pm 0.52	1.54 \pm 0.15	2.59 \pm 0.26	4.66	0.23	94.11 \pm 0.36	0.26	0.22 \pm 0.02	0.30	0.049
Point 5		1.10 \pm 0.29	1.01 \pm 0.10	2.12 \pm 0.21	4.66	0.23	94.11 \pm 0.36	0.26	0.41 \pm 0.04	0.31	0.049
Matrix grain 3											
Point 3		2.71 \pm 0.54	2.57 \pm 0.26	4.00 \pm 0.40	5.86	0.27	92.76 \pm 0.36	0.23	0.17 \pm 0.02	0.30	0.046
Point 4		1.91 \pm 0.69	1.77 \pm 0.18	3.23 \pm 0.32	5.75	0.27	92.14 \pm 0.36	0.27	0.15 \pm 0.02	0.29	0.047
Point 5		1.72 \pm 0.66	1.60 \pm 0.16	3.15 \pm 0.31	5.53	0.27	92.89 \pm 0.36	0.24	0.18 \pm 0.02	0.30	0.049
Matrix grain 4											
Point 1		1.10 \pm 0.87	1.49 \pm 0.15	2.88 \pm 0.29	5.55	0.27	93.26 \pm 0.36	0.43	0.17 \pm 0.02	0.38	0.049
Point 2		0.82 \pm 1.12	1.16 \pm 0.12	2.57 \pm 0.26	5.60	0.27	93.29 \pm 0.36	0.43	0.13 \pm 0.01	0.32	0.048
Point 3		2.25 \pm 0.53	1.96 \pm 0.20	3.11 \pm 0.31	5.00	0.25	94.04 \pm 0.36	0.31	0.14 \pm 0.02	0.30	0.050
CI value		0.486	0.481	0.990	1.10	0.502	19.04	2.66	0.145	0.122	0.046

^a The grain number in some cases is followed by a dash and another number (e.g., grain 3-2), this indicates that grain 3 was analyzed in more than one location (e.g., in 3-2, the 2 is spot 2).

^b Approximate 2σ errors: Ni = ± 0.10 ; Co = ± 0.04 ; Fe = ± 0.38 ; Cr = ± 0.04 ; P = ± 0.04 .

grains could retain siderophile element patterns generated by previous melting events or by condensation of metal onto a previous surface of the chondrule (see section 4.3). Thus, we have no compelling evidence that any of the metal grains we studied predate chondrule formation.

Although we have little direct evidence about the nature of the precursor material for CR2 chondrites, we note that plausible chondritic analogues such as the matrices of unequilibrated chondrites or the precursors of CI chondrites are highly oxidized (e.g., Brearley and Jones, 1998). Silicates in the chon-

drules we studied have very low FeO contents (Table 6). If the precursors were highly oxidized, then most of the original FeO was reduced to Fe metal during the melting event. To convert the large amount of FeO in these materials to Fe metal, an effective reducing agent is required. Two plausible reducing agents have been identified: C in chondrule precursors or nebular gas. Of these, C seems the most likely. The oxidized materials that are the most plausible analogues to chondrule precursors are rich in C (e.g., Kerridge, 1985). The C contents of the mesostases of reduced type I chondrules from Se-

Table 5. Major, minor, and trace element concentrations for metal grains from chondrules and matrix of Renazzo USNM 6226-3.^a

Sample	Rim or interior	Os $\pm 2\sigma$ (ppm)	Ir $\pm 2\sigma$ (ppm)	Pt $\pm 2\sigma$ (ppm)	Ni ^b (wt%)	Co ^b (wt%)	Fe ^b (wt%)	Cr ^b (wt%)	Au $\pm 2\sigma$ (ppm)	P ^b (wt%)	Co/Ni
Chondrule 1											
Grain 1	I	3.18 \pm 0.88	3.49 \pm 0.35	7.09 \pm 0.71	10.09	0.36	88.03	0.18	0.22 \pm 0.02	0.52	0.036
Grain 2	R	0.32 \pm 0.26	0.41 \pm 0.05	1.00 \pm 0.10	4.49	0.23	93.67	0.15	0.83 \pm 0.09	0.38	0.051
Grain 3	R	0.57 \pm 0.38	0.71 \pm 0.07	1.54 \pm 0.15	4.35	0.21	94.20	0.11	1.00 \pm 0.10	0.39	0.048
Grain 4	I	2.17 \pm 1.02	2.45 \pm 0.25	6.12 \pm 0.61	12.68	0.54	85.66	0.33	0.17 \pm 0.02	0.37	0.043
Grain 5	I	2.97 \pm 0.86	3.29 \pm 0.33	6.52 \pm 0.65	10.63	0.41	87.85	0.17	0.22 \pm 0.02	0.36	0.039
Grain 6	R	1.48 \pm 0.45	1.72 \pm 0.17	3.20 \pm 0.32	4.66	0.24	94.66	0.24	0.44 \pm 0.05	0.38	0.052
Chondrule 2											
Grain 1-1	I	2.39 \pm 0.48	2.25 \pm 0.23	4.38 \pm 0.44	5.32	0.25	93.76	0.13	0.81 \pm 0.08	0.22	0.047
Grain 1-2	I	1.49 \pm 0.43	1.34 \pm 0.15	2.73 \pm 0.27	5.08	0.24	93.64	0.11	0.80 \pm 0.09	0.22	0.047
Grain 4	I	1.54 \pm 0.35	1.53 \pm 0.15	3.62 \pm 0.36	5.17	0.24	94.32	0.12	1.26 \pm 0.13	0.20	0.046
Grain 5	I	1.49 \pm 0.30	1.73 \pm 0.17	3.68 \pm 0.37	5.15	0.26	94.42	0.14	0.60 \pm 0.06	0.27	0.050
Grain 6	I	1.78 \pm 0.38	1.85 \pm 0.19	3.60 \pm 0.36	5.27	0.28	93.10	0.13	0.52 \pm 0.05	0.24	0.053
Chondrule 3											
Grain 3-3	I	2.78 \pm 0.71	3.08 \pm 0.31	5.92 \pm 0.59	5.21	0.25	92.96	0.22	0.22 \pm 0.04	0.31	0.048
Grain 3-4	I	2.33 \pm 1.45	2.52 \pm 0.25	5.45 \pm 0.55	5.40	0.27	93.53	0.22	0.24 \pm 0.03	0.32	0.050
Chondrule 5											
Grain 1	I	2.18 \pm 0.91	2.17 \pm 0.22	4.05 \pm 0.41	5.88	0.29	91.83	0.29	0.18 \pm 0.02	0.26	0.049
Grain 2	I	2.61 \pm 0.52	2.40 \pm 0.24	4.24 \pm 0.42	5.22	0.25	92.28	0.31	0.16 \pm 0.02	0.33	0.048
Grain 3	I	1.75 \pm 0.13	2.14 \pm 0.21	4.91 \pm 0.49	5.56	0.30	92.07	0.29	0.13 \pm 0.02	0.27	0.054
Matrix grain 1											
Point 6		2.91 \pm 1.92	2.36 \pm 0.24	4.69 \pm 0.47	5.84	0.28	93.15	0.24	0.09 \pm 0.01	0.27	0.048
Point 7		2.51 \pm 1.16	2.23 \pm 0.22	4.29 \pm 0.43	6.68	0.31	92.43	0.26	0.09 \pm 0.01	0.21	0.046
Point 8		1.12 \pm 0.65	1.54 \pm 0.15	3.63 \pm 0.36	6.22	0.26	92.57	0.30	0.09 \pm 0.01	0.22	0.042
Point 9		1.57 \pm 1.48	1.81 \pm 0.18	3.16 \pm 0.32	5.54	0.24	93.68	0.24	0.11 \pm 0.01	0.21	0.043
Point 10		1.78 \pm 0.30	1.55 \pm 0.19	3.04 \pm 0.30	6.48	0.31	91.37	0.27	0.11 \pm 0.01	0.17	0.048
Matrix grain 2											
Point 1		0.39 \pm 0.69	0.45 \pm 0.05	1.14 \pm 0.11	4.65	0.32	94.45	0.23	0.11 \pm 0.01	0.26	0.069
Matrix grain 3											
Point 1		0.95 \pm 0.43	1.37 \pm 0.14	2.97 \pm 0.30	5.55	0.27	93.11	0.41	0.42 \pm 0.04	0.40	0.049
CI value		0.486	0.481	0.990	1.10	0.502	19.04	2.66	0.145	0.122	0.046

^a The grain number in some cases is followed by a dash and another number (e.g., grain 3-2); this indicates that grain 3 was analyzed in more than one location (e.g., in 3-2, the 2 is spot 2).

^b Approximate 2σ errors: Ni = ± 0.10 ; Co = ± 0.04 ; Fe = ± 0.38 ; Cr = ± 0.04 ; P = ± 0.04 .

markona (LL3.0), Bishunpur (LL3.1), and Allende (CV3) tend to be higher than those of the oxidized type 2 chondrules from the same meteorites (Hanon et al., 1998). Furthermore, metal grains in CR2 chondrites often have a thin layer of carbon on their surfaces (Kong et al., 1999). Experiments show the addition of C to chondrule analog compositions will, upon melting, produce metal and silicates that are analogous, both in composition and texture, to those found in chondrules from unequilibrated chondrites (Connolly et al., 1994). However, experiments that rely on reduction by exchange between molten synthetic chondrules and gas mixtures (CO-CO₂; H₂-CO) have not been successful in reproducing the compositions and textures of metal and silicates (Tsuchiyama, and Miyamoto, 1984; Connolly, 1996; Cohen et al., 2000a,b). The presence of C as a reducing agent in chondrule precursors appears critical to production of most Fe-Ni metal observed in chondrules.

The amount of carbon needed to act as a reducing agent within chondrule precursors can be estimated. Iron and Ni are by far the most important elements to be reduced. We assume that Fe and Ni existed as FeO and NiO in the starting material and were present in CI abundances. If C is oxidized to CO₂, then the amount of C necessary to reduce all of the FeO and NiO to Fe and Ni is ~ 2.2 wt%. If Fe is entirely present as Fe₂O₃, then a C content of 3.2 wt% is required. If FeO and NiO are entirely reduced by C to produce CO, then ~ 4.4 wt% C is

required. We note that CI chondrites and the matrices of CM2 chondrites contain 3 to 4 wt% C (Kerridge, 1985). The C contents of other unequilibrated chondrites imply that their matrixes are similarly rich in C (e.g., Kerridge, 1985; Jarosewich, 1990). Thus, it is plausible that sufficient C could have been present in the precursors of CR2 chondrite chondrules for Fe-Ni metal to have formed in situ through reduction by the oxidation of C while the chondrules were molten. Experiments indicate that reduction of FeO to Fe metal by oxidation of C takes place very quickly (e.g., minutes) upon melting at high temperatures (e.g., 1500 to 1700°C; Connolly et al., 1994).

There are mineralogical consequences for chondrules in which a CI abundance of FeO has been reduced to metal. FeO is a major constituent of olivine and orthopyroxene. Reduction of FeO to Fe metal removes this constituent from the silicate melt and thus increases the proportion of SiO₂ in the melt. By increasing the degree of silica saturation, reduction of FeO can result in an increased abundance, or even the appearance of modal orthopyroxene in the chondrule. Thus, the role of reduction and Fe loss from chondrule may have a direct effect in producing the various kinds of type I chondrules. We do not advocate that this process was the only one controlling the mineralogy of the chondrules. As already discussed, it is likely that some evaporation occurred and potentially both these

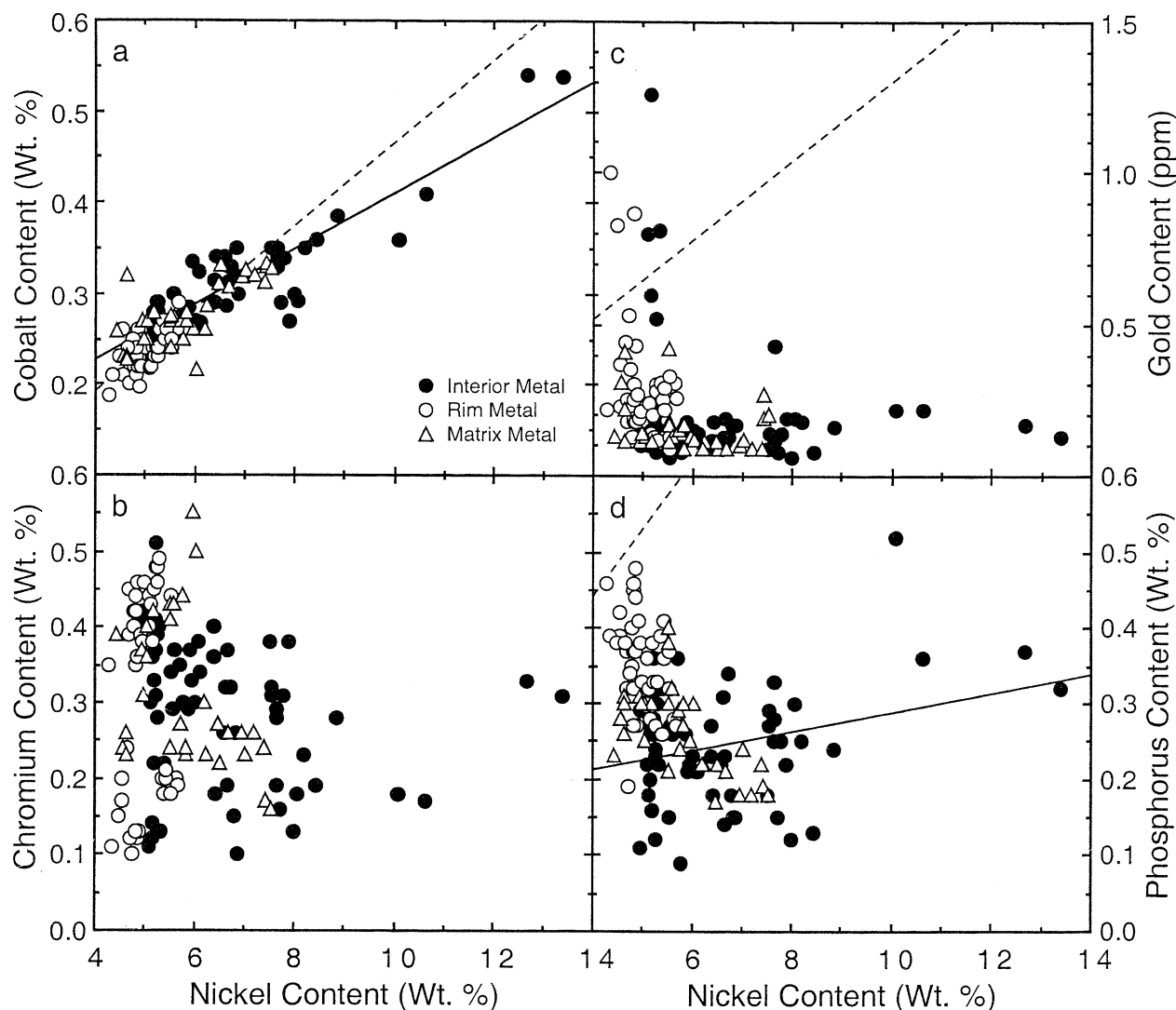


Fig. 5. Contents of several elements vs. Ni content of Fe-Ni metal grains from all three meteorites. Error bars are all slightly larger than the symbols and are not plotted. (a) Co vs. Ni. Interior grains have slightly higher Co and Ni contents than rim grains, although the two populations overlap between 5 and ~ 7.5 wt% Ni. The solid line shows a regression through the data and the dashed line show the solar Co/Ni ratio. (b) Cr vs. Ni. Chromium contents of rim, interior, and matrix grains span a similar range, although rim metal has two populations, Cr rich and Cr poor. (c, d) Au vs. Ni and P vs. Ni. Gold and P in most grains are depleted relative to the solar abundance. Rim grains tend to have higher Au and P abundances than interior grains, whereas matrix grains cover most of the observed range.

processes were complicated by multiple heating events. The main point is that metal production within, and loss of metal from, chondrules is likely an important mechanism for fractionating bulk chondrule compositions.

4.3. Volatile Depletions and Recondensation of Evaporated Metal

Although some metal on chondrule rims is similar to that in chondrule interiors, much of the rim metal is strongly depleted in Os, Ir, and Pt relative to interior metal, and many rim grains are enriched in Au and P relative to interior metal (Figs. 6 to 9). Some matrix grains have similar characteristics (Fig. 10). The fact that most of these refractory-depleted grains are located

either on chondrule rims or in the matrix suggests that they formed by condensation of siderophile elements from a refractory-poor reservoir during or after chondrule formation. Depletion of refractory elements could have been caused by earlier condensation of these elements at higher temperatures, followed by physical removal of the condensates from the gas phase. However, such a model cannot explain the depletions of Au and P relative to CI abundances or the enrichments of these same elements compared with that found in metal from chondrule interiors. The abundances of Au and P indicate that the vapor phase from which the metal recondensed was depleted in Au and P relative to CI abundances. This implies that material from which the vapor phase originated was also depleted in Au and P. Depletions of Au and P in all of the bulk chondrules

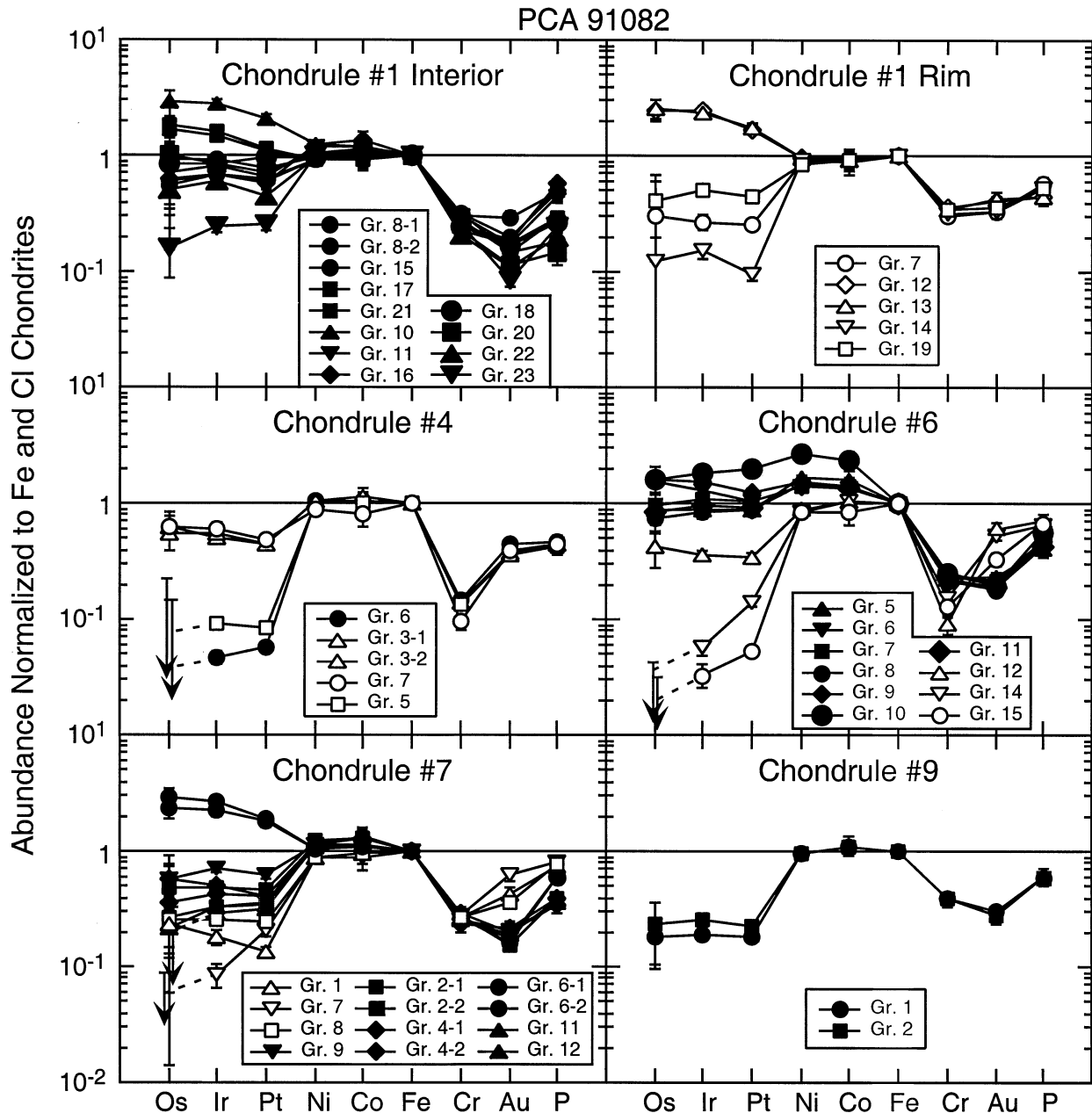


Fig. 6. Siderophile–element abundances relative to Fe (x-axis), normalized to the same ratios for a CI composition (sample element/sample Fe/CI element/CI Fe; y-axis) for metal associated with chondrules 1, 4, 6, 7, and 9 from PCA 91082. Closed symbols represent metal from chondrule interiors, and open symbols are for metal on chondrule rims. The horizontal line represents the cosmic ratio. Arrows indicate upper limits on the measured Os value. Element volatility increases from left to right.

studied suggest that the chondrule melts themselves were the source of the siderophiles in the vapor from which the metal condensates formed.

Chondrule melts existed at sufficiently high temperatures that so Au and P, and probably Fe, Ni, and Co, would have been rapidly lost via evaporation. We infer from the fact that metal was retained in the chondrules that the duration of the melting event was of short (minutes to a few hours above 1783 K). Partial evaporation of volatiles from chondrule melts at

temperatures >1783 K would result in significant loss of Au and P, some loss of Fe, Ni, and Co, and almost complete retention of Os, Ir, and Pt. The remaining metal in the solids would have somewhat higher $R_{PGE/Fe}$ than CI (grains in the interiors of PCA chondrules 1, 7, and 8; EET chondrules 1; Renazzo chondrules 1; Figs. 6 to 9). The resulting vapor phase would have very low $R_{PGE/Fe}$ values and higher $R_{vol-Sid/Fe}$ than the molten chondrule. Condensates from such a vapor would have similar fractionated ratios. That fact that all grains have

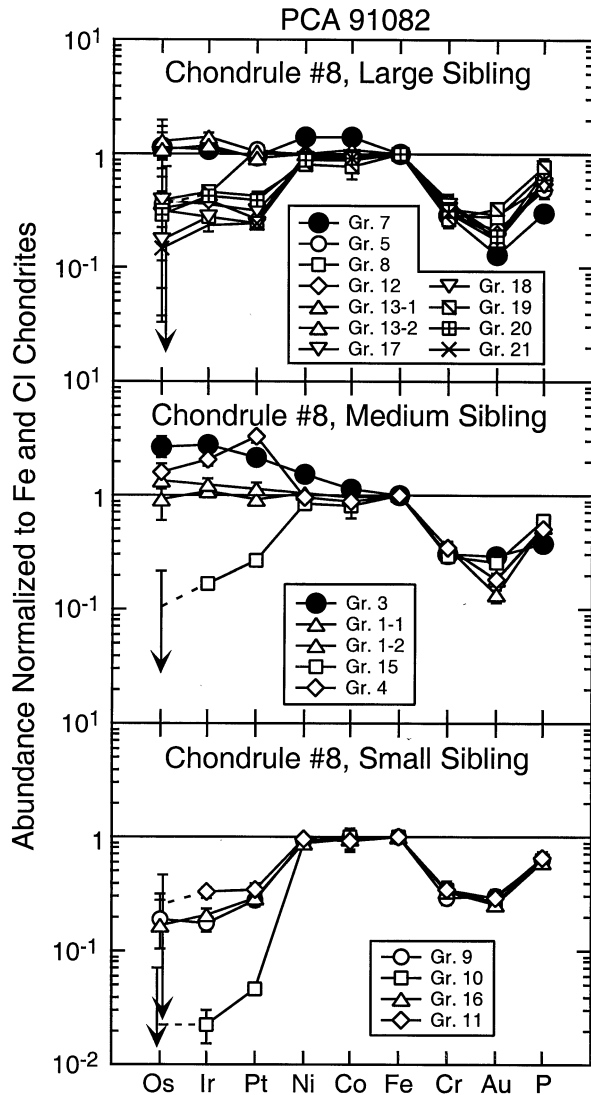


Fig. 7. Siderophile–element ratios for metal associated with components of compound chondrule 8 from PCA 91082. Figure format and symbols as in Figure 6.

some refractory PGEs probably indicates that metal formed by reduction acted as nucleation sites for the condensing metal. Grains formed by condensation from a cooling vapor might be expected to show compositional zoning, with the last to condense being richest in the most volatile elements and most depleted in refractory elements. There is a hint that some of the large matrix grains are zoned. For example, EET grain 2 shows larger depletions of refractory PGEs near the edges than in the interior (Fig. 10). Unfortunately, the 10- μm spatial resolution used in this study we did not resolve fine zoning in metal grains. Annealing or remelting the metal grains would also eliminate compositional zoning.

The formation of chondritic metal by vapor deposition has been considered previously. In their study of Renazzo, Kong et al. (1999) and Kong and Palme (1999) concluded that observed fractionations in the abundances of volatile siderophile elements between matrix, chondrules, and chondrule rims are the

result of the chondrule-forming process. During this process volatile elements evaporated from chondrules and recondensed onto materials that formed the chondrite matrix. Other workers have proposed that some metal in CH and related chondrites formed by condensation from a gas phase on the basis of trace-element abundances (Meibom et al., 1999, 2000; Campbell et al., 2000). Furthermore, one recent experimental study has revealed that vapor deposition of euhedral metal crystals on the surfaces of chondrules is consistent with metal condensation on chondrule surfaces (Reisener et al., 2000; J. I. Goldstein, personal communication), adding further support for our vapor deposition model.

4.4. Model for the Production of CR2 Chondrules

From the above considerations, it follows that the role of vapor phases must be considered in the formation of chondrules and that there will be a relationship between condensed and vapor phases. However, it is widely recognized that chondrules cannot form as direct condensates from a hot nebular region of solar composition at any plausible range in pressures (e.g., Yoneda and Grossman, 1995; Ebel and Grossman, 2000). Neither liquid Fe nor silicate melts derived from chondritic composition are stable under these conditions. In condensation calculations, hydrogen only serves as a reducing agent and a dilutant of the condensable species. It follows that the conditions under which chondrules formed must have involved a process that produced reduced Fe and where the pressures of the “condensable elements” were sufficient to permit chondrule melts and Fe metal liquid to survive until the chondrule forming process was over. Pressures must also have been sufficiently high to permit significant amounts of more volatile elements to recondense onto cooling chondrules. We assume that the dust concentration and gas pressure (from all components) were far above those of the canonical nebula. The gas phase that is considered to have been present when the chondrules formed had dominant contributions from the evaporation of preexisting solids and, to some extent, from the chondrules themselves. The details of the interaction between the gas phase and the chondrules are not well constrained. We note that equilibrium calculations have been done at high dust to gas ratios that go in the direction we indicate here (e.g., Yoneda and Grossman, 1995; Ebel and Grossman, 2000). However, theoretical calculations for the nonequilibrium systems considered here do not currently exist in the literature. We further consider that while there was interaction between the chondrules and the vapor, the f_{O_2} of the chondrules was controlled internally in a transient regime involving carbon (solid) as a reducing agent and not H_2 . In this view, nebular gas did not play a significant role. The presence of molten Fe metal in the chondrule melts and the compositions of the metal and associated silicates place strict constraints on the temperature and f_{O_2} of the melt.

Conceptually, we envision an environment consisting of dust and a coexisting gas phase containing volatile elements evaporated from the dust. The system is considered to be of bulk “cosmic” composition. The dust, which was rich in carbon, aggregated together into clumps and was melted by transient heating events. The FeO was reduced to metal in the molten droplets by the carbon inherited from the dust. Metal was

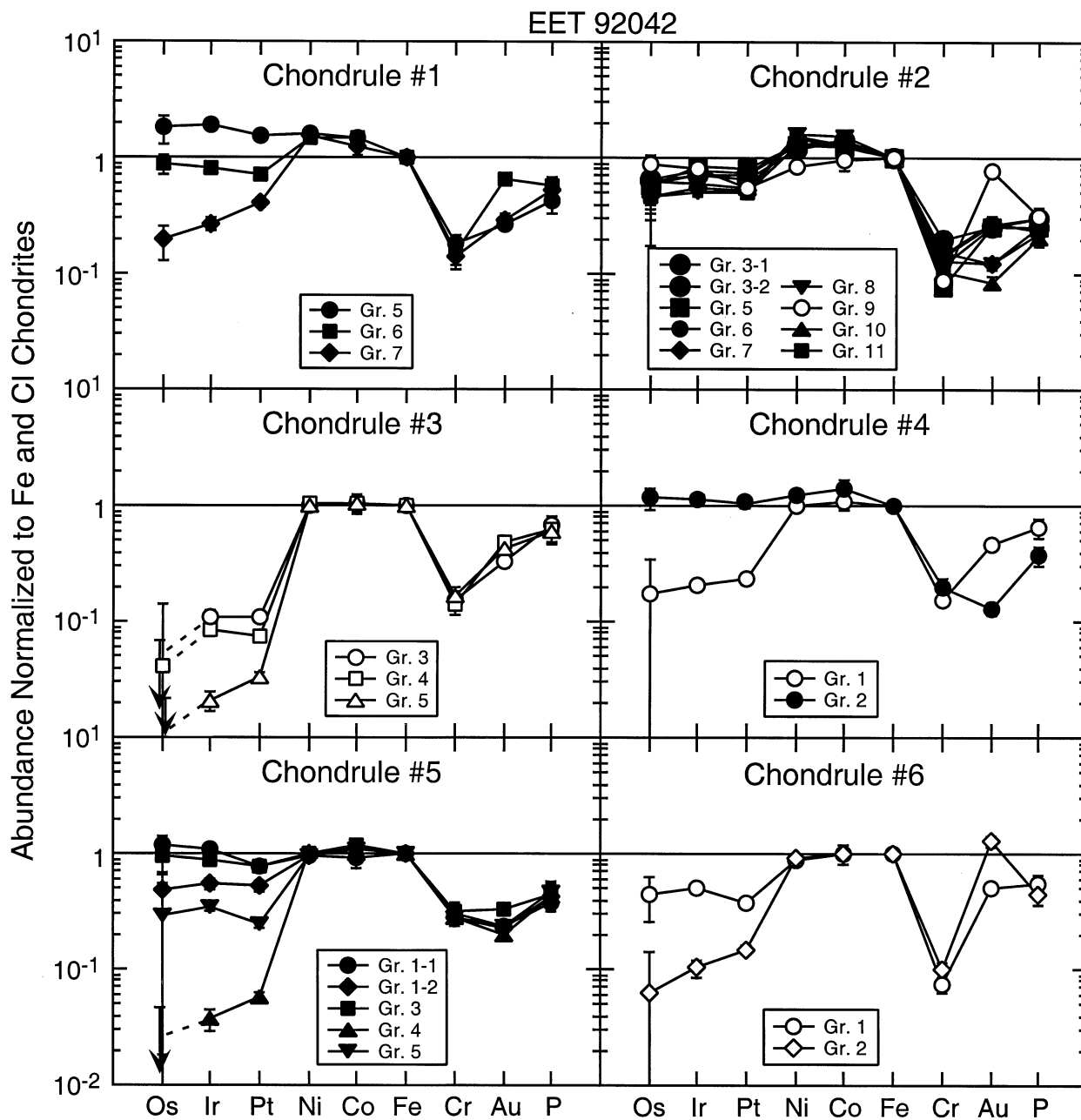


Fig. 8. Siderophile–element ratios for metal associated with chondrules 1, 2, 3, 4, 5, and 6 from EET 92042. Figure format and symbols as in Figure 6.

expelled and volatile elements were lost from the chondrules during their brief existence as melt droplets. As the chondrules rapidly cooled and solidified, volatile elements recondensed onto their surfaces. The final chondrules then reflect the melting processes and the surface reactions with the coexisting vapor phase.

Here we consider simple models for the origin of the observed fractionation patterns of Fe, Os, Ir, Pt, Au, and P in the metal phase and the elemental abundances of bulk chondrules. We assume that all the Fe was originally present as FeO in the

chondrules and was reduced by carbon during the melting event with, in some cases, a portion of it evaporated before or during reduction within the melt. We describe the basic elemental patterns to be found in chondrules that retain or lose Fe and detail the relationships to be found for the bulk composition of the chondrule relative to their initial assumed CI abundances. We also compare the ratios $R_{X/Fe}$ of element X to Fe metal to the known ratios in CI meteorites. The symbol $R_{PGE/Fe}$ is used to represent the PGEs, and $R_{Vol-Sid/Fe}$ represents the volatile siderophiles.

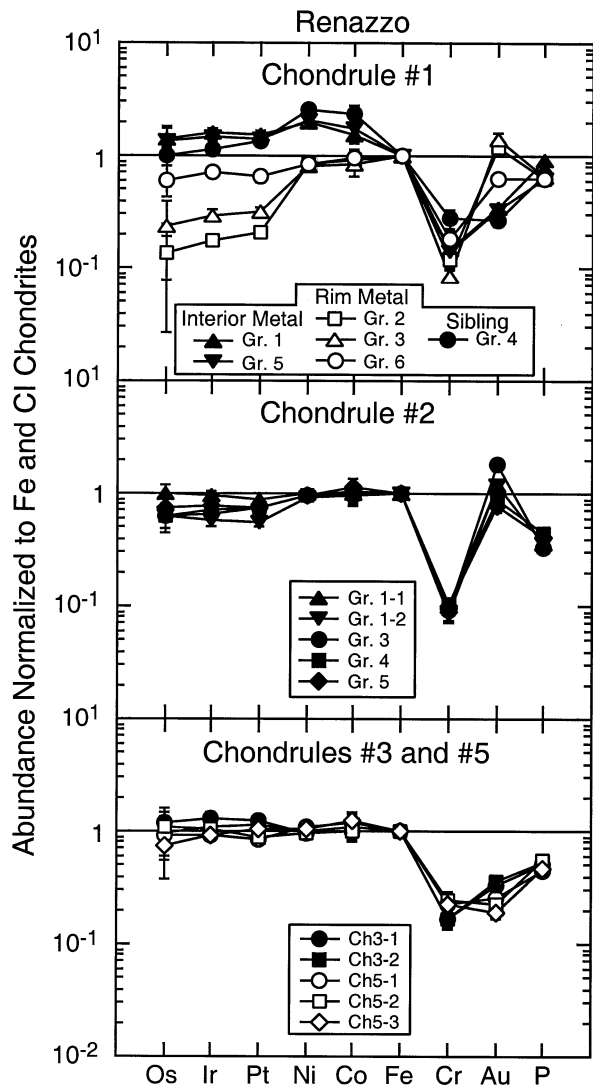


Fig. 9. Siderophile–element ratios for metal associated with chondrules 1, 2, 3, and 5 from Renazzo. Only interior metal is shown for chondrules 2, 3, and 5, and rim metal for chondrule 1 is identified in the legend. Figure format as in Figure 6.

4.4.1. Case 1

We assume that elements more refractory than Cr are present in the proportions of bulk CI meteorites and volatile elements are depleted at a consistent level, for simplicity ignoring differences in the temperature dependence of their individual volatilities (which we also assume for each case discussed below). The bulk abundance pattern of a chondrule with these characteristics would be as shown in the filled symbols in Figure 14A. Elements more refractory than Cr exhibit a flat pattern when normalized to CI values and plot just slightly above the CI line. If Fe were completely reduced to metal and all the siderophile elements were extracted by the metal from the silicate melt, the resulting metal would have ratios of Os/Fe, Ir, Fe, and Pt/Fe ($R_{PGE/Fe}$), equal to the CI ratios and lower Au/Fe and P/Fe ratios ($R_{vol-Sid/F}$) reflecting the lower Au and P abundances in the precursor (filled squares in Fig. 14B).

4.4.2. Case 2

Case 2 is the same as case 1, except we assume that some Fe metal is expelled from the chondrule. The remaining metal would have the same values of $R_{Sid/Fe}$ and $R_{vol-Sid/F}$, as in case 1. However, the bulk chondrule would have siderophile element abundances shifted to lower values, and the remaining lithophile elements would be enriched compared with CI abundances, as shown by open symbols in Figure 14A. The expelled metal would have the same values of $R_{X/PGE}$ as that remaining in the chondrule.

4.4.3. Case 3

In case 3, we model metal production as a two-stage process. (1) In the first stage, a small amount of Fe was reduced to metal and that metal extracted the bulk of the siderophile elements from the chondrule. The resulting metal would have $R_{PGE/Fe}$ and $R_{vol-Sid/F}$ far above CI ratios with relatively lower $R_{vol-Sid/F}$ reflecting the volatile-depleted initial composition (filled diamonds in Fig. 14B). (2) As the rest of the Fe was reduced to metal and the two stages of metal were homogenized, the $R_{PGE/Fe}$ and $R_{vol-Sid/F}$ ratios of the metal would become the same as in the starting material (filled squares in Fig. 14B). (3) However, if the first metal were kept segregated, then the second batch of Fe would be highly depleted in siderophiles (open circles in Fig. 14B). The only way the second batch of metal would contain significant siderophiles would be if the first generation metal had access to only a fraction of the total siderophile inventory. To preserve such a difference, the generations of metal would have to be kept out of diffusive communication with each other. If no Fe metal were expelled, then the chondrule would have a bulk elemental abundance pattern, as in case 1. If metal were expelled, the bulk elemental abundance pattern of the chondrule would be as in case 2. The expelled metal would exhibit $R_{PGE/Fe}$ as in the segregated metal of the two stages.

4.4.4. Case 4

If a chondrule experienced more extensive volatile loss, including some Cr, Mg, Si, and Fe and their associated oxygen, the remaining refractory elements, both lithophile and siderophile, would be enhanced in the bulk composition (filled circles, Fig. 15a). b If the remaining Fe were reduced to metal, the resulting metal would have $R_{PGE/Fe} \gg R_{CI}$, but $R_{vol-Sid/Fe} < R_{CI}$ (Fig. 15b). If this metal were expelled from the chondrule, the bulk composition would be depleted in siderophiles, as shown by the filled squares in Figure 15a. If the metal were formed in two stages, the results would be analogous to those outlined for case 1 above, but with the siderophile-element patterns discussed here.

In all of the above cases, in the absence of a fractionating mechanism, the elements Os, Ir, and Pt should track each other with relative proportions given by the CI abundances. As shown above, the CI-normalized abundances of refractory elements depend strongly on the amount of Fe (metal) retained in the chondrule. The amounts of modal Fe metal in the chondrule interiors are given in Figures 11 to 13. Chondrules that have lost no Fe should contain ~21.5 wt% metal.

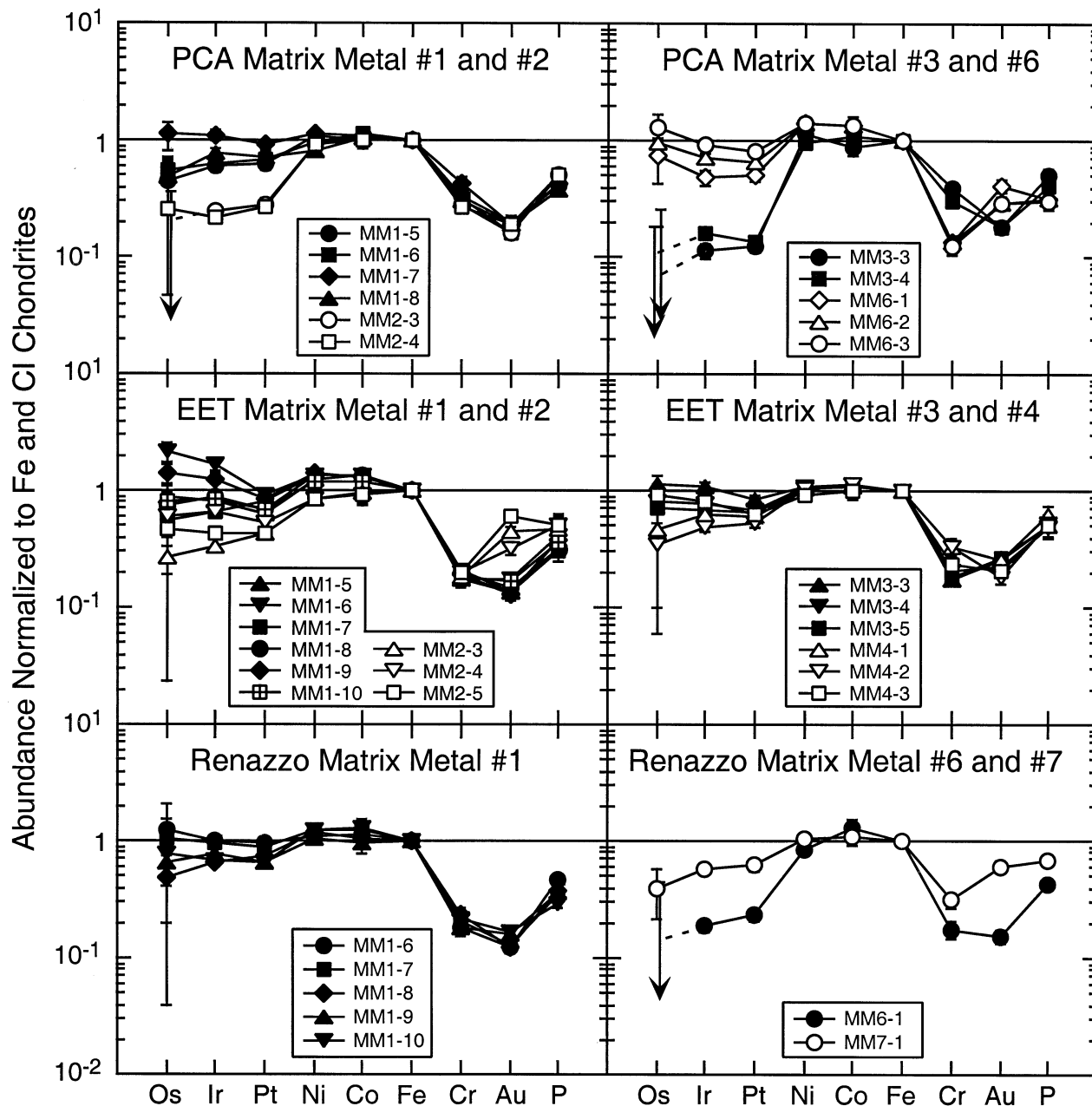


Fig. 10. Siderophile–element ratios for isolated matrix metal grains from all three meteorites. MM = matrix metal, which is followed by a grain number and an analysis number (e.g., MM1-5 means grain 1, analysis 5). Figure format and symbols as in Figure 6.

4.5. Comparison with the Observations

We now compare the observations with the simplified model presented above. It must be remembered that the modal abundances have relatively large uncertainties, particularly with regard to obtaining a representative sample of metal globules in and around the chondrules. Examples of chondrules that are not depleted in Fe and refractory siderophiles (simple form of case 1 above) include PCA chondrules 1 and 7 and EET chondrule 1 (Figs. 11 and 12). These chondrules have high metal abundances near that expected for a CI compo-

sition (~21.5 wt%) and do not appear to have expelled much metal. The high metal and siderophile–element abundances in PCA chondrules 1 and 7 relative to expectations for a CI composition probably reflect an inaccurate modal metal abundance due to the large metal grains present in the section that we measured. Alternatively these chondrules could have experienced more than one episode of heating. All three of these chondrules show large variations in $R_{PGE/Fe}$ that require multiple stages of metal formation, with the products kept essentially isolated from each other. Dif-

Table 6. Averaged analyses of silicates and mesostasis from investigated chondrules.^a

	Na ₂ O	MgO	Al ₂ O ₃	SiO ₂	CaO	TiO ₂	Cr ₃ O ₃	MnO	FeO	Total
PCA 91082,15										
<i>Chondrule 1</i>										
Olivine	na	55.27	0.06	41.51	0.19	bd	0.50	0.06	1.93	99.52
Mesostasis	0.17	2.61	27.18	49.62	17.51	0.52	0.26	0.05	1.73	99.65
Low-Ca Pyx	0.02	36.95	0.85	57.49	0.59	bd	0.79	0.26	1.83	98.78
High-Ca Pyx	bd	7.12	13.15	61.93	10.32	1.78	0.72	0.17	2.95	98.14
<i>Chondrule 4</i>										
Olivine	na	52.33	0.07	40.57	0.23	bd	0.37	0.19	2.84	96.60
Lo-Ca-Pyx	^b bd	34.94	0.36	56.45	0.36	^b bd	0.93	0.43	3.21	96.68
High-Ca Pyx	0.09	23.33	2.81	52.62	10.91	0.36	2.00	2.02	2.44	96.58
<i>Chondrule 6</i>										
olivine	na	55.44	0.07	42.46	0.28	bd	0.53	0.14	1.58	100.49
Mesostasis	0.16	16.90	12.97	51.24	16.03	0.55	0.96	0.18	1.35	100.34
Low-Ca Pyx	0.05	36.59	0.80	57.97	0.73	bd	0.79	0.25	2.88	100.06
High-Ca Pyx ^b	0.09	21.58	2.65	51.11	11.94	0.33	1.88	1.84	3.85	95.27
<i>Chondrule 7</i>										
Olivine	na	54.79	0.14	40.99	0.25	bd	0.60	0.17	2.34	99.28
Mesostasis	0.94	5.70	21.10	53.26	14.18	0.71	0.63	0.27	2.35	99.14
Low-Ca Pyx	bd	38.28	0.93	57.23	0.40	bd	0.69	0.10	1.67	99.30
High-Ca Pyx	0.03	18.11	8.55	49.93	18.96	bd	1.99	0.33	0.82	98.72
<i>Chondrule 8L</i>										
Olivine	na	56.04	0.20	42.88	0.44	bd	0.22	bd	0.97	100.82
Mesostasis	1.86	6.00	22.38	55.17	13.30	0.51	0.51	0.48	0.86	101.07
Low-Ca Pyx	bd	37.35	1.00	58.89	0.46	0.14	0.88	0.12	1.79	100.64
High-Ca Pyx	0.05	17.68	8.19	49.05	18.73	0.97	2.29	0.49	2.54	99.98
<i>Chondrule 8m</i>										
Olivine	na	55.39	0.04	42.87	0.23	bd	0.61	0.14	1.67	100.97
Mesostasis	1.33	5.25	23.30	54.55	13.57	0.47	0.47	0.39	1.09	100.42
Low-Ca Pyx	bd	38.78	0.48	59.95	0.36	0.08	0.67	0.10	0.93	101.35
High-Ca Pyx ^b	0.04	18.33	9.17	49.86	18.38	0.99	2.46	0.48	0.86	100.57
<i>Chondrule 8s</i>										
Olivine	na	55.63	0.20	42.60	0.31	bd	0.38	<0.03	1.35	100.53
Mesostasis ^c	3.02	4.51	22.00	56.34	11.64	0.45	0.60	1.47	0.76	100.76
High-Ca Pyx ^b	0.11	14.99	9.33	46.08	19.31	1.33	3.32	1.85	3.58	99.90
<i>Chondrule 9</i>										
Olivine ^c	na	55.83	0.04	42.74	0.16	0.03	0.56	0.07	1.34	100.77
Mesostasis ^b	2.74	1.76	18.66	64.23	7.37	0.22	0.12	0.37	1.29	96.76
Low-Ca Pyx	bd	38.02	0.66	59.13	0.46	0.09	0.64	0.15	1.36	100.51
EET 92042,20										
<i>Chondrule 1</i>										
Olivine	na	54.56	0.05	41.72	0.20	bd	0.77	0.70	2.91	100.91
Mesostasis	0.91	2.08	31.61	45.70	16.44	0.03	0.06	0.06	2.42	99.31
Low-Ca Pyx	bd	36.86	0.90	58.88	0.59	0.11	0.78	0.40	2.42	100.94
High-Ca Pyx	<0.02	30.59	3.15	56.14	5.89	0.80	1.54	0.92	2.20	101.25
<i>Chondrule 2</i>										
Olivine	na	54.86	0.02	41.76	0.19	bd	0.57	0.19	2.97	100.56
Mesostasis ²	0.69	9.07	19.35	49.30	14.76	0.73	1.04	0.51	4.54	99.98
Low-Ca Pyx	bd	37.70	0.97	57.87	0.38	0.15	0.82	0.15	2.78	100.82
High-Ca Pyx	0.03	17.46	7.79	47.19	18.11	0.91	3.03	0.54	1.50	96.56
<i>Chondrule 3</i>										
Olivine	na	54.72	0.16	41.75	0.30	bd	0.69	0.21	3.25	101.08
Mesostasis	0.34	0.8	31.83	48.99	17.58	0.02	0.02	bd	0.39	99.97
Low-Ca Pyx	bd	36.56	1.26	56.33	0.73	0.07	0.87	0.12	2.66	98.60
<i>Chondrule 4</i>										
Olivine	na	55.91	bd	42.46	0.19	bd	0.59	0.12	1.86	101.13
<i>Chondrule 5</i>										
Olivine	na	55.59	0.07	41.74	0.20	bd	0.75	0.18	2.05	100.58
Mesostasis	0.40	5.33	21.88	56.72	14.36	0.59	0.48	0.19	0.91	100.86
High-Ca Pyx	bd	17.37	9.46	50.15	20.07	1.13	2.35	0.19	0.81	101.53
<i>Chondrule 6</i>										
Olivine	na	53.47	0.14	41.74	0.21	bd	0.66	0.44	4.53	101.19
Mesostasis	2.18	4.19	23.82	53.59	12.64	0.60	0.20	0.48	2.42	100.12
Low-Ca Pyx	bd	37.52	0.54	57.33	0.38	0.03	0.81	0.30	2.84	99.75
High-Ca Pyx	0.05	19.14	8.15	50.78	17.20	0.76	2.27	0.61	2.20	101.16

(Continued)

Table 6. (Continued)

	Na ₂ O	MgO	Al ₂ O ₃	SiO ₂	CaO	TiO ₂	Cr ₃ O ₃	MnO	FeO	Total
Renazzo USNM 6226-3										
<i>Chondrule 1</i>										
Olivine	na	55.73	0.10	41.75	0.36	bd	0.38	0.14	1.93	100.38
Mesostasis	1.22	3.92	23.89	55.18	12.41	0.56	0.27	0.31	1.07	98.83
Low-Ca Pyx	bd	37.89	1.00	57.27	0.34	0.13	0.88	0.16	1.94	99.61
High-Ca Pyx	0.06	17.70	9.70	49.09	18.43	1.03	2.49	0.70	1.24	100.43
<i>Chondrule 2</i>										
Low-Ca Pyx ^b	bd	35.72	0.25	56.81	0.19	bd	0.51	0.29	3.47	97.24
<i>Chondrule 3</i>										
Low-Ca Pyx ^c	bd	35.94	0.48	57.00	0.25	0.05	0.92	0.22	2.69	97.55
<i>Chondrule 5</i>										
Low-Ca Pyx	bd	38.27	0.62	59.22	0.34	0.10	0.76	0.14	1.38	100.83
Mesostasis ^c	1.28	11.45	18.62	50.31	13.74	0.62	1.34	0.66	2.02	100.04

^a Each reported value is an average of at least three analyses of the cores of three different grains (or areas for mesostasis).

^b Either only one grain could be located or only one yielded acceptable data.

^c This is an average of two different grains either because only two could be found or only two yielded acceptable data.

bd = Below detection limit; na = not available.

ferent amounts of PGE must have been locally available to the different Fe metals formed.

In contrast to this group of chondrules, there are four chon-

drules that are grossly depleted in Fe and siderophiles (PCA chondrule 8, large and medium siblings; EET chondrules 3 and 6; and Renazzo chondrule 1). All show corresponding deple-

Table 7. List of the bulk composition of selected chondrules we investigated from modal recombination. All values are in ppm unless otherwise designated.

Sample	PCA Ch1	PCA Ch7	PCA Ch8L	PCA Ch8M	EET Ch1	EET Ch2	EET Ch3	EET Ch6	REN Ch1
Na (wt%)	0.07	0.04	0.08	0.03	0.02	0.65	0.01	0.08	0.03
Rb	0.44	0.57	1.05	1.25	1.28	1.37	1.56	1.62	3.37
P (wt%)	0.08	0.09	0.01	0.01	0.07	0.53	0.01	0.01	0.01
Mn (wt%)	0.03	0.09	0.08	0.12	0.33	0.15	0.12	0.33	0.12
Au	0.04	0.05	0.01	0.01	0.07	0.05	0.001	0.001	0.01
Cr (wt%)	0.33	0.41	0.35	0.44	0.43	0.42	0.50	0.47	0.39
Fe (wt%)	37.40	34.44	66.51	44.28	24.48	34.06	3.08	4.30	4.52
Mg (wt%)	17.45	17.66	24.59	29.69	20.83	13.36	25.89	27.31	27.06
Si (wt%)	12.25	13.15	22.01	20.09	16.39	14.63	22.64	20.79	21.43
Co (wt%)	0.13	0.14	0.03	0.01	0.11	0.15	0.01	0.01	0.02
Ni (wt%)	2.16	2.16	4.65	2.83	2.03	2.56	0.06	0.08	0.40
Pt	1.57	1.28	0.28	0.36	1.06	1.06	0.05	0.07	0.23
U	0.02	0.01	0.02	0.01	0.01	0.04	0.01	0.01	0.01
Ba	2.56	3.62	5.25	2.15	2.78	8.58	1.49	4.51	0.33
Sr	9.01	9.72	13.53	5.25	4.63	21.07	8.24	12.18	0.45
Ca (wt%)	1.23	1.35	1.29	0.92	0.67	2.48	1.02	1.36	0.94
Ti (wt%)	0.03	0.04	0.07	0.04	0.02	0.11	0.02	0.05	0.05
Nb	0.38	0.47	0.61	0.29		0.67	0.27	0.49	0.46
La	0.22	0.29	0.40	0.17	0.26	0.70	0.19	0.35	0.28
Ce	0.58	0.81	1.07	0.48	0.69	1.77	0.49	0.93	0.72
Pr	0.09	0.11	0.14	0.08	0.10	0.26	0.06	0.13	0.11
Nd	0.45	0.56	0.67	0.36	0.41	1.16	0.29	0.65	0.49
Sm	0.13	0.16	0.20	0.12	0.12	0.36	0.08	0.22	0.13
Eu	0.06	0.06	0.08	0.03	0.04	0.14	0.05	0.08	0.04
Gd	0.23	0.28	0.27	0.17	0.19	0.54	0.16	0.32	0.18
Tb	0.04	0.04	0.05	0.03	0.03	0.10	0.02	0.06	0.03
Dy	0.27	0.32	0.33	0.24	0.19	0.60	0.17	0.37	0.21
Y	1.75	1.84	2.17	1.64	1.23	3.68	1.09	2.24	1.34
Ho	0.06	0.07	0.07	0.06	0.04	0.14	0.04	0.08	0.05
Er	0.23	0.23	0.27	0.18	0.16	0.42	0.14	0.27	0.17
Tm	0.03	0.03	0.03	0.03	0.03	0.07	0.02	0.04	0.03
Yb	0.16	0.22	0.26	0.19	0.16	0.47	0.15	0.27	0.20
Lu	0.03	0.03	0.05	0.03	0.02	0.07	0.02	0.04	0.03
Th	0.02	0.04	0.07	0.03	0.03	0.08	0.03	0.06	0.04
Ir	0.93	0.75	0.16	0.13	0.57	0.53	0.03	0.03	0.11
Sc	11.90	12.17	23.93	18.76		16.70	20.76	18.60	21.21
Al (wt%)	1.35	1.26	1.46	0.74	0.82	2.40	1.25	1.35	0.94
Zr	4.99	5.23	7.10	3.71	4.21	9.58	3.22	6.00	5.18
Os	0.95	0.76	0.16	0.22	0.56	0.46	0.03	0.04	0.10

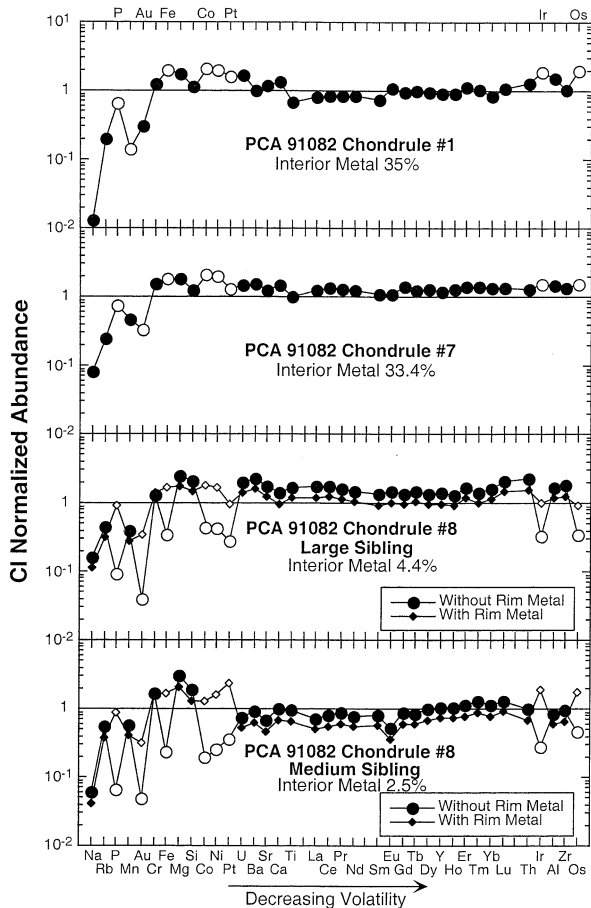


Fig. 11. Bulk compositions of chondrules 1, 7, and 8 from PCA 91082 normalized to CI abundance. Open symbols are for siderophile elements. Elements are plotted with decreasing volatility from left to right. Note the unfractionated patterns and roughly CI abundances for elements more refractory than ~Cr in each chondrule. Elements more volatile than Cr show varying degrees of depletion. For the two siblings of compound chondrule 8, the bulk compositions were calculated in two ways: including the rim metal, and without the rim metal. Note the nearly flat elemental pattern when the rim siderophiles are added to the large sibling. The calculated overabundance of siderophile elements in the medium sibling probably indicates an incorrect mode (see section 2.4).

tions in the PGE elements, and all have low modal metal abundances (Figs. 11 to 13). These chondrules appear to follow case 2. Interior metal was observed in only two of the chondrules (PCA chondrule 8 and Renazzo chondrule 1), and both have $R_{PGE/Fe}$ values equal to or higher than CI (Figs. 7 and 9). The higher $R_{PGE/Fe}$ values could indicate a late extraction of all remaining siderophiles in the melt. In all of the cases discussed so far (assigned to cases 1 and 2), the volatile siderophiles Au and P are severely depleted relative to any effects observed in Os, Ir, and Pt. PCA chondrule 8 has a large amount of rim metal, some of which has $R_{PGE/Fe}$ and $R_{vol-Sid/Fe}$ that are unfractionated with respect to CI ratios (Fig. 7). If the mode for this chondrule is recalculated to include rim metal, the abundances of Fe and siderophile elements are no longer depleted in the large sibling and appear to be enriched in the medium sibling (probably due to an unrepresentative mode). These

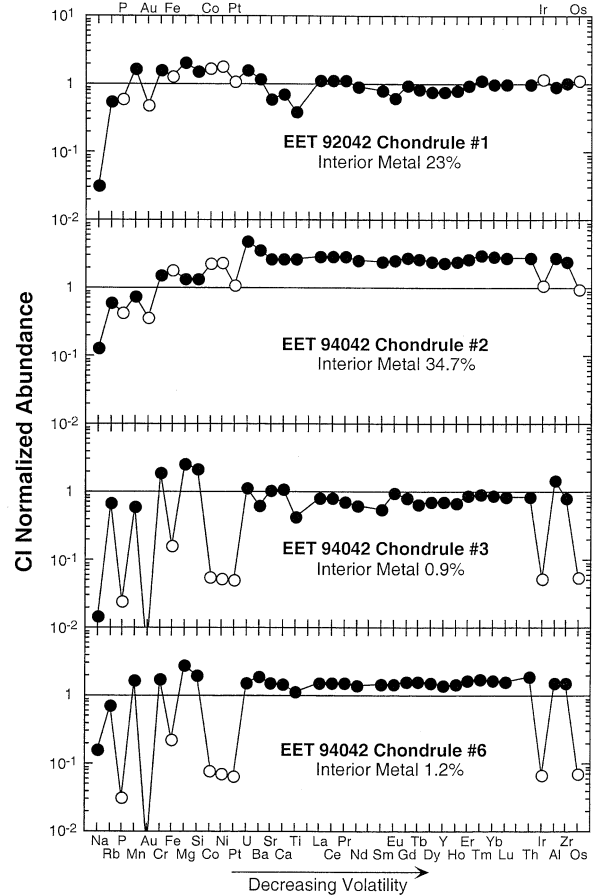


Fig. 12. Bulk compositions of chondrules 1, 2, 3, and 6 from EET 92042 normalized to CI abundances. Open symbols are for siderophile elements. Again note the unfractionated patterns and near-CI abundances of the elements more refractory than ~Cr and variable depletions of volatiles. For chondrule 3, we were unable to analyze a metal grain from its interior. We have therefore used the composition of interior grains from metal-rich chondrules to estimate the bulk siderophile content of chondrule 3.

patterns strongly suggest that much of the rim metal on PCA chondrule 8 came from the interior of the chondrule (also see Fig. 1). In contrast, rim metal from EET chondrules 3 and 6 and

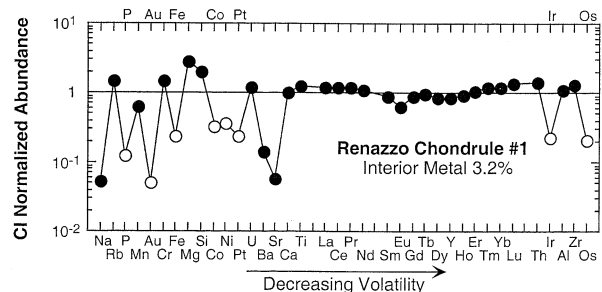


Fig. 13. Bulk composition of chondrule 1 from Renazzo normalized to CI abundance. Open symbols are for siderophile elements. Large depletions in Ba and Sr probably reflect leaching of these elements from the mesostasis.

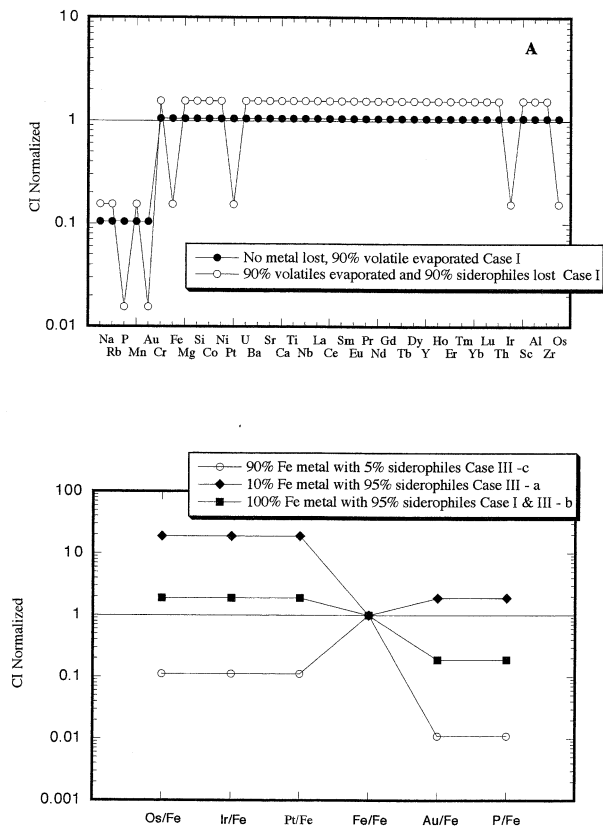


Fig. 14. Model calculations of how chondrule bulk compositions and the siderophile element patterns of metal grain within chondrules vary on the basis of the loss of elements, metal, and the partitions on siderophile elements into metal. (A) We model the bulk composition of a chondrule assuming its precursor, premelting bulk composition was CI. Volatility increases to the left. First, 90% of the volatile elements Au, Mn, P, Rb, and Na are lost as a result of evaporation upon heating of the precursor chondrule, producing almost an order of magnitude decrease in volatiles but only a slight increase in lithophile elements more refractory than Au above CI abundances. (B) The ratioed siderophile abundance patterns for metal grains within a chondrule. These are simple calculations that assume that 90% of Au, Mn, P, Rb, and Na are lost as a result of evaporation and that the metal has no Ni or Co. One model (filled circles) assumes that 90% of the FeO was converted to Fe-metal and contains 5% of the siderophile elements. Next (filled diamonds), we assume that only 10% of the FeO was converted to metal but that it contains 95% of the siderophiles. Finally, we assume that 100% of the FeO was reduced to Fe metal and 95% of the siderophile elements were partitioned into this metal.

Renazzo chondrule 1 is depleted in refractory PGEs and relatively enriched in Au and P (Figs. 8 and 9). We consider this behavior to be directly associated with rim metal and to be due to the addition of volatile-rich metal from interactions with a vapor phase, with the interior metals being isolated from the rim metal.

One chondrule, EET chondrule 2, shows substantial enrichments of refractory lithophiles relative to CI abundances. However, Cr, Mg, and Si are not enriched as much and Fe is also relatively depleted. This chondrule is most closely approximated by case 4 described above, where substantial Cr, Fe, Mg, and Si were lost through evaporation and some metal was expelled from the chondrule (cf. Figs. 12 and 15a). The side-

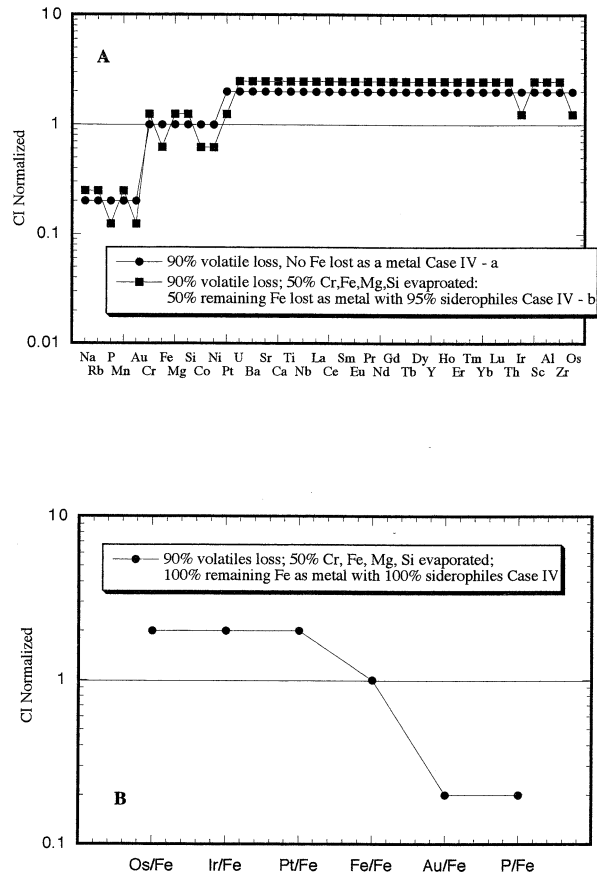


Fig. 15. Model calculations for how chondrule bulk compositions and the siderophile element patterns of metal grain within chondrules vary on the basis of the loss of elements, metal, and the partition of siderophile elements into metal. (A) A similar plot to Fig. 14A, but here, after losing 90% of the volatile element to evaporation, we then lose 50% of the Cr, Fe, Mg, and Si to evaporation. This increases lithophile elements more refractory than Si to 2x CI abundances. Next, we follow the procedure of (A) but reduce 50% of the remaining FeO to Fe, partition 95% of the siderophile elements into this metal, and then expel or remove the metal with its siderophiles from the chondrule. The effect is to increase elements more refractory than Si to slightly above 2x CI and to deplete all the siderophiles by nearly 2x. (B) Metal grain with its siderophile element content. Here, we model a 90% loss of volatiles and 50% of Cr, Fe, Mg, and Si as a result of evaporation. We then reduce 100% of the remaining FeO to Fe and partition 100% of the siderophile elements into this metal.

rophile-element pattern of EET chondrule 2 is somewhat depleted in refractory PGEs (Fig. 8), which suggests either that early-formed metal enriched in PGEs was expelled from the chondrule or that some recondensation of volatiles into the chondrule occurred.

5. CONCLUSIONS

Our study has identified two basic types of metal in CR2 chondrites. One type, found within chondrule interiors, their rims, and as isolated grains within the matrix, has $R_{\text{PGE/Fe}}$ values that vary coherently between $\sim 2x$ CI and $\sim 0.2x$ CI, with most grains having $R_{\text{PGE/Fe}}$ close to CI values. This metal also has solar Ni/Fe and Co/Fe ratios and is depleted in Cr, Au,

and P relative to CI (i.e., low $R_{\text{vol-Sid/Fe}}$). These metal grains most likely formed by reduction of FeO within the chondrule melts. Carbon in the precursor material was the likely reducing agent. The molten Fe-metal melt efficiently extracted the siderophile elements from the bulk chondrule silicate melts. The molten metal was immiscible with the surrounding silicate melts. Metal was ejected from many chondrule melts producing variable depletions in the bulk siderophile element content of some chondrules. Some molten metal droplets were trapped within the chondrules when they solidified. Grains trapped at chondrule surfaces are now preserved as rim metal. The low abundances of Au and P in this group of grains are due in part to a general depletion of volatiles in the chondrule precursors and in part to evaporative loss during the chondrule-melting event. Many of the metal droplets expelled from chondrules are now preserved as one group of isolated matrix metal grains.

The second type of metal grains, found both on chondrule rims and as isolated matrix grains, typically has much lower $R_{\text{PGE/Fe}}$ values than solar ratios, approximately solar Ni/Fe and Co/Fe, and higher $R_{\text{vol-Sid/Fe}}$ values than interior metal. This metal probably formed by condensation from vapors that had evaporated from chondrules during their formation. Elements that vaporize at temperatures near or above the chondrule-melting temperature mostly remained in the chondrules, whereas the more volatile elements evaporated with efficiencies reflecting their vaporization temperatures. As the gas cooled, these elements recondensed onto chondrule surfaces to become rim grains and into isolated metal grains to become matrix grains. Chondrules with multistage histories exhibit both types of metal within their complex structures.

The newly developed SIMS technique that we used to measure the trace-element contents of the individual metal grains (Hsu et al., 2000) has provided a means of getting detailed compositional information on chondrite metal grains while preserving their petrologic context. A preliminary study of ordinary chondrites has shown complexity similar to that described here for unequilibrated meteorites (Hsu et al., 1998b). The technique is also useful for understanding the distribution of PGEs and Au among minerals of iron meteorites (Hsu et al., 2000). Clearly, this new SIMS technique is applicable to the study of Fe-Ni metal and sulfides in a range of planetary materials.

Acknowledgments—We thank D. Papanastassiou, R. Ash, B. Zanda, R. Jones, S. Russell, and J. Beckett for helpful discussions. We thank B. Zanda, J. Wasson, A. Meibom, and H. Palme for constructive reviews. We are especially grateful to B. Zanda for many helpful discussions and comments that improved the quality of this article. We thank the Meteorite Working Group for the loan of thin sections of two Antarctic meteorites. This work was supported by NASA NAG5-4319 (H.C.C.; D. S. Burnett, principal investigator), NAG5-8158 (G.R.H.), and NAG5-4083 (G.J.W.). Caltech Division contribution 8725(1056).

Associate editor: H. Palme

REFERENCES

- Armstrong J. T. (1995) CITZAF—A package of correction programs for the quantitative electron microbeam X-ray-analysis of thick polished materials, thin-films, and particles. *Microbeam Anal.* **4**, 177–200.
- Brearley A. J. and Jones R. H. (1998) Chondritic meteorites. In *Planetary Materials* (ed. J. J. Papike), pp. 3–1–3–398. Reviews in Mineralogy 36. Mineralogical Society of America.
- Campbell A. J. and Humayun M. (1999a) Trace element microanalysis in iron meteorites by laser ablation ICP-MS. *Anal. Chem.* **71**, 939–946.
- Campbell A. J. and Humayun M. (1999b) Microanalysis of platinum group elements in iron meteorites using laser ablation ICP-MS. *Lunar. Planet. Sci.* **30**, 1974.
- Campbell A. J., Humayun M., Meibom A., Krot A. N., and Keil K. (2001) Origin of metal grains in the QUE94411 chondrite. *Geochim. Cosmochim. Acta* **65**, 163–180.
- Cohen B., Yu Y., Hewins R. H., and Zanda B. (2000a) Opaque-rich chondrules: Not due to the canonical nebular gas? *Lunar. Planet. Sci.* **31**, 1212.
- Cohen B., Hewins, R. H., and Yang Y. (2000b) Evaporation in the young solar nebula as the origin of “just-right” melting of chondrules. *Nature* **406**, 600–602.
- Connolly H. C. Jr. (1996) Carbon, nebular gas, and reduced chondrule formation: Experimental investigation. *Meteorit. Planet. Sci.* **31**, A30–A31.
- Connolly H. C. Jr., Hewins R. H., Ash R. D., Zanda B., Lofgren G. E., and Bourout-Denise M. (1994) Carbon and the formation of reduced chondrules. *Nature* **371**, 136–139.
- Connolly H. C. Jr., Huss G. R., Hsu W., and Wasserburg G. J. (1998) Formation of chondrule and matrix metal within CR2 meteorites as constrained from their PGE abundances. *Lunar Planet. Sci. Conf.* **29**, abstract 1548.
- Connolly H. C. Jr., Huss G. R., and Wasserburg G. J. (2000) On the formation of metal in CR2 chondrites: In situ determination of PGE distributions and bulk chondrule compositions. *Lunar Planet. Sci. Conf.* **31**, 1437.
- Ebel D. S. and Grossman L. (2000) Condensation in dust-enriched systems. *Geochim. Cosmochim. Acta* **64**, 339–366.
- Fahey A. J., Goswami J. N., McKeegan K. D., and Zinner E. K. (1987) ^{26}Al , ^{244}Pu , ^{50}Ti , REE and trace element abundances in hibonite grains from CM and CV meteorites. *Geochim. Cosmochim. Acta* **51**, 329–350.
- Gooding J. L. and Keil K. (1981) Relative abundance of chondrule primary textural types in ordinary chondrites and their bearing on conditions of chondrule formation. *Meteoritics* **16**, 17–43.
- Grossman J. N., Rubin A. E., Nagahara H., and King E. A. (1988) Properties of chondrules. In *Meteorites and the Solar System* (eds. J. F. Kerridge and M. S. Matthews), pp. 619–659. University of Arizona Press.
- Hanon P., Robert F., and Chaussidon M. (1998) High carbon concentrations in meteoritic chondrules. *Geochim. Cosmochim. Acta* **62**, 903–913.
- Hsu W., Huss G. R., and Wasserburg G. J. (1998a) In situ ion probe measurements of PGEs and their distributions between metallic phases of irons. *Lunar Planet. Sci.* **29**, 1781
- Hsu W., Huss G. R., and Wasserburg G. J. (1998b) In situ ion probe measurements of PGEs and their distributions between metallic phases of chondrites. *Lunar Planet. Sci.* **29**, 1939.
- Hsu W., Huss G. R. and Wasserburg G. J. (2000) Ion probe measurements of Os, Ir, Pt, and Au in individual phases of iron meteorites. *Geochim. Cosmochim. Acta* **64**, 1133–1147.
- Jarosewich E. (1990) Chemical analyses of meteorites: A compilation of stony and iron meteorite analyses. *Meteoritics* **24**, 323–337.
- Jones R. H. (1994) Petrology of FeO-poor, porphyritic pyroxene chondrules in the Semarkona chondrite. *Geochim. Cosmochim. Acta* **54**, 5325–5340.
- Jones R. H. (1996) Relict grains in chondrules: Evidence for recycling. In *Chondrules and the Protoplanetary Disk* (eds. R. H. Hewins, R. H. Jones, and E. R. D. Scott), pp. 163–172. Cambridge University Press.
- Jones R. H. and Scott E. R. D. (1989) Petrology and thermal history of chondrules in the Semarkona (LL3.0) chondrite. *Proc. Lunar Planet. Sci. Conf.* **19**, 523–536.
- Jones R. H. and Danielson L. R. (1997) A chondrule origin for dusty relict olivine in unequilibrated chondrites. *Meteorit. Planet. Sci.* **32**, 753–760.
- Kallemeyn G. W., Rubin A. E. and Wasson J. T. (1994) The compo-

- sitional classification of chondrites: VI. The CR carbonaceous chondrite group. *Geochim. Cosmochim. Acta* **58**, 2873–2888.
- Kerridge J. F. (1985) Carbon, hydrogen and nitrogen in carbonaceous chondrites: Abundances and isotopic compositions of bulk samples. *Geochim. Cosmochim. Acta* **49**, 1707–1714.
- Kong P. and Palme H. (1999) Compositional and genetic relationship between chondrules, chondrule rims, metal, and matrix in the Renazzo chondrite. *Geochim. Cosmochim. Acta* **63**, 3673–3682.
- Kong P., Ebihara M., and Palme H. (1999) Distribution of siderophile elements in CR chondrites: Evidence for evaporation and recondensation during chondrule formation. *Geochim. Cosmochim. Acta* **63**, 2637–2652.
- Kracher A., Scott E. R. D., and Keil K. (1983) Relict and other anomalous grains in chondrules: Implications for chondrule formation. *Proc. Lunar. Planet. Sci. Conf. 14th (Part 2) J. Geophys. Res. Suppl.* **89**, B559–B566.
- Larimer J. W. and Anders E. (1970) Chemical fractionations in meteorites—III. Major element fractionations in chondrites. *Geochim. Cosmochim. Acta* **34**, 367–387.
- Lee M. S., Rubin A. E., and Wasson J. T. (1992) Origin of metallic Fe-Ni in Renazzo and related chondrites. *Geochim. Cosmochim. Acta* **56**, 2521–2533.
- Meibom A., Krot A. N., Petaev M. I., Wood J. A., and Keil K. (1999) Primitive FeNi metal grains in CH carbonaceous chondrites formed by condensation from a gas of solar composition. *J. Geophys. Res. Planets* **104**, 22053–22059.
- Meibom A., Desch S. J., Krot A. N., Cuzzi J. N., Petaev M. I., Wislon L., and Keil K. (2000) Large-scale thermal events in the solar nebula: Evidence from Fe, Ni metal grains in primitive meteorites. *Science* **288**, 839–841.
- Nagahara H. (1981) Evidence for secondary origin of chondrules. *Nature* **292**, 135–136.
- Planner H. N. (1986) Appearance of metal at the chondrule surface during chondrule melting. *Meteoritics* **21**, 484–485.
- Rambaldi E. R. (1981) Relict grains in chondrules. *Nature* **293**, 558–561.
- Reisener R., Meibom A., Krot A. N., Goldstein J. I., and Keil K. (2000) Microstructure of condensate Fe-Ni metal particles in the CH chondrite PAT91546. *Lunar Planet. Sci.* **31**, 1445.
- Shen J. J., Papanastassiou D. A., and Wasserburg G. J. (1996) Precise Re-Os determinations and systematics of iron meteorites. *Geochim. Cosmochim. Acta* **60**, 2887–2900.
- Swartzendruber L. J., Itkin E. P., and Alcock C. B. (1991) The Fe-Ni (iron-nickel) system. *J. Phase Equil.* **12**, 288–312.
- Tsuchiyama A. and Miyamoto M. (1984) Metal grains in chondrules: An experimental study. *Lunar. Planet. Sci.* **15**, 868–869.
- Wasson J. T. (1985) *Meteorites—Their Record of Early Solar-System History*. W. H. Freeman.
- Weisberg M. K., Prinz M., Clayton R. N., and Mayeda T. K. (1993) The CR (Renazzo-type) carbonaceous chondrite group and its implications. *Geochim. Cosmochim. Acta* **57**, 1567–1586.
- Weisberg M. K., Prinz M., Clayton R. N., Mayeda T. K., Grady M. M., and Pillinger C. T. (1995) The CR chondrite clan. *Proc. NIPR Symp. Antarct. Meteorites* **8**, 11–32.
- Yoneda S. and Grossman L. (1995) Condensation of CaO-MgO-Al₂O₃-SiO₂ liquids from cosmic gases. *Geochim. Cosmochim. Acta* **59**, 3413–3444.
- Zanda B., Bourot-Denise M., Perron C., and Hewins R. H. (1994) Origin and metamorphic redistribution of silicon, chromium, and phosphorus in the metal of chondrites. *Science* **265**, 1846–1849.
- Zinner E. K. and Crozaz G. (1986) Ion probe determinations of the abundances of all the rare earth elements in single mineral grains. In *Secondary Ion Mass Spectrometry (SIMS V)* (ed. A. Benninghoven et al.), pp. 444–446. Springer-Verlag.